



Transverse Project in Manufacturing

Project Report

Joint Master in Manufacturing 4.0

NAME

WISEMAN SIRIRO

Ecole Centrale de Lyon, France

Master of Science in Mechanical Engineering and Advanced Technologies

Instructors:

Prof. Carbol ÉLODIE

Prof. Alexey SOVA

Prof. Maria DUBENSKAYA

Prof. Frederic VALIORGUE

Prof. Cederic COURBON

Prof. Federic CABANETTE

Contents

1	Introduction	1
2	Powder Characterization	2
2.1	Introduction.....	2
2.2	Objectives	2
2.3	Powder Types and Manufacturing Processes	2
2.4	Flowability.....	2
2.5	Apparent and Tap Density	3
2.6	Morphology.....	4
2.7	Material Characterization.....	7
2.8	Conclusions.....	10
3	Laser Cladding	11
3.1	Introduction.....	11
3.2	Objectives	11
3.3	Material and Parameters.....	11
3.4	Coating characterization.....	13
3.5	Results and Discussion.....	13
3.6	Conclusions.....	18
4	Belt Finishing	20
4.1	Introduction.....	20
4.2	Objectives	21
4.3	Materials and Methods	21
4.4	Result and Discussion.....	23
4.5	Conclusions.....	26
5	Ball Burnishing	28
5.1	Introduction.....	28
5.2	Objectives	28
5.3	Materials and Method	29
5.4	Results and Discussion.....	30
5.5	Conclusion	36
6	Surface Topography Characterization	37
6.1	Introduction.....	37
6.2	Objectives	38
6.3	Material and Methodology.....	38
6.4	Results and Discussion.....	40
6.5	Conclusion	44
7	Conclusion	45
8	References	46
A	Appendix A title	48
A.1	Surface Topography Characterization.....	48



1 | Introduction

This comprehensive report delves into the techniques and processes explored over the course of the semester. The initial section zeroes in on the analysis of the most pivotal element in additive manufacturing: the powder. The subsequent section provides insight into the effects of depositing 316L stainless steel powder through laser cladding and cold spray deposition. The third and fourth chapters delve into the application of belt finishing and ball burnishing post-processing techniques to the laser-clad samples. Finally, the 3D topography of the samples is examined using non-contact methods to study the surface parameters and identify the distinct process signatures.



2 | Powder Characterization

Authors: Cesar Villatoro, Cheong Yoo, Ever Cente, Junaid Ali, Neel Ghag

2.1 | Introduction

Powder Characterization and Testing are essential for gaining a thorough understanding of the physical and technological properties of powders, contributing to the optimization of processes and the assurance of quality outcomes. This report investigates key aspects of powders, including flowability, density, morphology, and chemical composition, aiming to provide comprehensive.

2.2 | Objectives

This study aims to conduct a thorough comparison between spheroidized and non-spheroidized powders by analyzing their flowability, tap density, morphology, and chemical composition. Flowability testing will assess the ease of powder flow, while tap density measurements will evaluate packing efficiency. Morphological analysis will examine particle size distribution and shape consistency, utilizing SEM imaging and laser diffraction. Chemical composition will be compared using SEM-EDS to quantify elemental makeup and distribution. This comprehensive approach will provide valuable insights into the physical, morphological, and chemical properties of the powders, aiding in informed decision-making for diverse industrial applications.

2.3 | Powder Types and Manufacturing Processes

The two powders that are studied in this paper are: non-spheroidized and spheroidized Ti6Al4V alloy.

- **Non spheroidized powder (NS)** has been manufactured using the Gas Atomization technology; a process that takes a melted sample of a metal alloy and creates a melt stream. The melt stream is then impinged with a powerful atomization gas that causes dispersion and creates particles. The particles or droplets then fall and cool as they make contact with a substrate or metal plate [1]. This method involves the conversion of liquid metal into fine powder particles through the use of a high-velocity gas stream. The process is commonly used for the production of metal powders with specific characteristics, including spherical shapes and a narrow size distribution [2].
- **Spheroidized powder (S)** has been produced by Plasma Spheroidization; this process begins with gas atomization, where molten metal is atomized into fine droplets using a high-velocity gas stream, which is then introduced into a chamber where it comes into contact with a high-temperature plasma torch, after that, the plasma flame is directed onto the incoming powder particles. The extreme heat generated by the plasma torch causes rapid heating of the powder. As the molten material moves through the plasma flame, surface tension forces act to round off irregularities and reshape the particles into more spherical forms. Once the particles pass through the plasma flame, they cool and solidify into spherical or near-spherical shapes. The rapid cooling helps to "freeze" the improved spherical morphology. [3] Powders fabricated by PS have many advantages such as high spheroidization ratio, narrow size distribution and good flowability, which make it the most ideal method to fabricate spherical Ti6Al4V powder [4].

2.4 | Flowability

The flowability of a powder stands as a pivotal element influencing the effectiveness of Additive Manufactured parts. Powder exhibiting favorable flowability ensures even spreading, resulting in greater stability in the performance of the molded product. Factors such as powder morphology, particle size distribution, and moisture content significantly contribute to flowability. For this study, a titanium alloy (Ti-6Al-4V) in two different conditions was studied: not spheroidized (prepared by gas atomization) and spheroidized (prepared by plasma spheroidization). For measuring the flowability of the powders, we used a Hall funnel following the ASTM B 213 standard for metallic powders [5]. This procedure was followed: a 50-gram dry sample of the powder is introduced into the funnel, with the orifice initially manually blocked with the fingertip. Upon removing the fingertip, the stopwatch is initiated, and the timing concludes right when the final particles exit the funnel. The flowability of the sample is denoted as the time in seconds required

for 50 g of the powder to pass through the orifice (s/50 g). In Figure 2.1 the Hall funnel used for the flowability measurement can be observed.



Figure 2.1: Hall funnel for flowability measurement

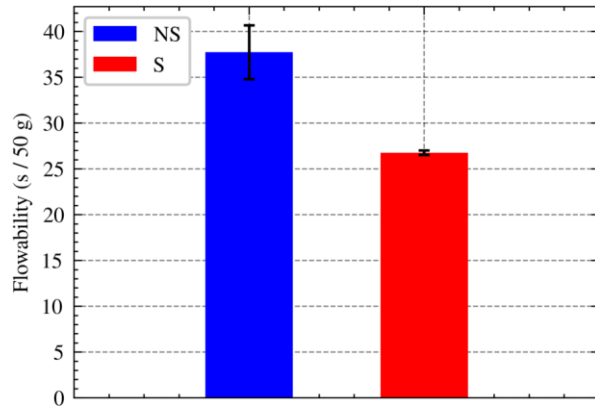


Figure 2.2: Flowability measured for Ti-6Al-4V powders (NS and S)

The results obtained by the measurement are displayed in Figure 2.2. The non-spheroidized powder is denoted by NS and the spheroidized powder is denoted by S. A different value of flowability is observed for both powders, with the spheroidized powder having a better flowability (see Table 2.1).

Table 2.1: Flowability values and its measurement error

Powder	Flowability (s/50 g)
Ti-6Al-4V (NS)	37.736 ± 2.935
Ti-6Al-4V (S)	26.760 ± 0.255

We can see that the spheroidized powder has a better flowability (lower value), this means that the powder flows more easily and quickly through an orifice, reflecting better handling characteristics and improved efficiency which is beneficial for various manufacturing processes.

2.5 | Apparent and Tap Density

Apparent density is the mass of a powder per unit volume (g/cm^3), considering the total volume occupied by the powder particles and the void spaces between them. Apparent density of a metal powder strongly depends on the particle size. Usually, it decreases with decreasing particle size, and it also decreases as the particle shape becomes more irregular. For powders exhibiting a broad spectrum of particle sizes, the apparent density tends to rise as the gaps between larger particles get occupied by smaller particles. In the other hand, tap density refers to the density of a powder when it has been tapped into a container under specific conditions. Essentially, it quantifies how closely the particles of the powder pack together after tapping. Tap density is a function of particle size distribution, particle shape, and surface roughness. Tap density is always higher than the free-flow apparent density and it helps assess the flowability, compressibility, and handling characteristics of powders. For measuring the apparent density, a Hall funnel was also used following the standard ASTM B 212. The procedure consisted in placing 50 grams of powder in a graduated glass cylinder of 100 cm^3 and the volume of the powder was measured for calculating the apparent density using Equation 2.1. For the tap density in the other hand, the graduated cylinder with the powder was placed in a tapping apparatus (Figure 2.3) following standard ASTM B 527. The evolution of the volume with respect to the number of taps was measured and the Equation 2.1 was also used for calculating the tap density for each number of taps [5].

$$TD = \frac{M}{V} \quad (2.1)$$

The results for both not spheroidized and spheroidized powder (NS and S) can be seen in Figure 2.4. Note that apparent density is equal to tap density without any taps. As we can observe, the tap destiny is

increasing in both powders for each number of taps. 3000 is the final number of taps measured as it has been proven to be efficient for finding the final tap density. We can also observe a difference between both powders, where the spheroidized one has a higher apparent and tap density.



Figure 2.3: Tapping apparatus for measuring tap density

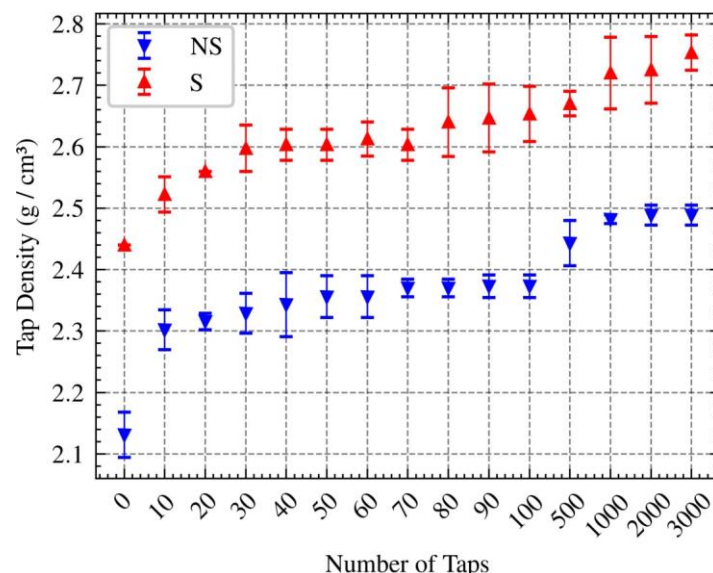


Figure 2.4: Tap density measured for Ti-6Al-4V powders (NS and S)

Additionally, compressibility index/Carr's index and Hausner ratio was calculated for characterizing the flowability (packing factor) in both powders. The results for all the measurements can be seen in Table 2.2.

Table 2.2: Apparent and Tap densities measured and its packing factor

Powder	Apparent density (g/cm³)	Tap density (g/cm³)	Carr's index (%)	Hausner ratio	Flowability
Ti-6Al-4V (NS)	2.131 ± 0.037	2.489 ± 0.016	14.37	1.17	Good
Ti-6Al-4V (S)	2.440 ± 0.000	2.753 ± 0.029	11.38	1.13	Good

As we can observe, both powders (NS and S) have good flowabilities according to their Carr's indexes and Hausner ratios. However, the powder that has been spheroidized has better packing factor. This means that powder particles can move easier and more uniformly, allowing for a smooth and consistent flow. Also, it means that the powder particles can rearrange themselves with less resistance and occupy a more compact arrangement during tapping.

2.6 | Morphology

Particle image analysis is used for the measurement of particle size, characterization of particle shape and morphological analysis. Optical microscopy serves as a highly precise method for particle image analysis, enabling the observation and measurement of individual particles. Advanced techniques such as scanning electron microscopy and transmission electron microscopy facilitate the analysis of nano and smaller particles. ASTM Standard E20 provides details on using optical microscopy for particle sizing. In our particle image analysis method, a precise quantity of the powder sample is carefully measured and deposited onto the observational mirror of a microscope. To ensure uniform spreading of the powder across the mirror's surface, vacuum technology (Figure 2.5) was employed to create a controlled environment. This vacuum facilitates the even distribution of the particles, eliminating clumping or uneven distribution that could compromise the accuracy of the analysis. The analysis is conducted using a microscope, and the resulting data is meticulously recorded and observed through specialized software. This systematic approach enhances the accuracy and reliability of the particle image analysis process, ensuring comprehensive insights into the powder's characteristics.

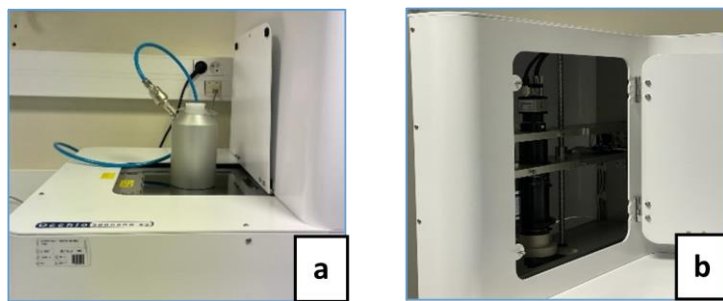


Figure 2.5: a) Vacuum system for particle uniform spreading b) Microscope for particle image analysis

2.6.1 | Particle size distribution analysis

Particle size distribution analysis is a technique used to determine the range of sizes present in a sample of particles. These measurements involve determining the sizes of particles, which are then utilized to categorize the two-dimensional images of particles based on an equivalent spherical particle. Although there are different ways of measuring the size of a particle explained by Eric Olson [6] (Figure 2.6). For the area-equivalent diameter refers to the diameter of a circle having the same area as the projected area of the particle. In other words, it represents the diameter of a circle that covers the same amount of area as the irregularly shaped particle when viewed from a certain perspective. This parameter is commonly used in particle size analysis to simplify the representation of particle sizes.

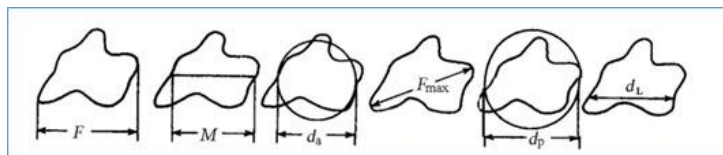


Figure 2.6: Measuring of irregular particles [5]

Figure 2.7 and Figure 2.8 showed the diameters and cumulative size distributions for gas atomized (NS) and spheroidized (S) powders. The box plot and error bars with standard deviation are plotted for the three datasets to uncertainty and distribution of result of experiments using python. For both powders the particle size range was found to be between $5\mu\text{m}$ and $115\mu\text{m}$ while the mean particle size was found to be $35\mu\text{m}$. The cumulative curves showed that both powders contain 50% of the $<40\mu\text{m}$. From the box plots and error bars, it can be observed that an improvement is seen in the estimation of the true particle size of S powder. This indicates that spheroidized particles exhibit a more regular shape, leading to increased measurement consistency and reduced variability, resulting in smaller error bars. This contrast highlights the importance of particle shape on measurement precision in powder characterization.

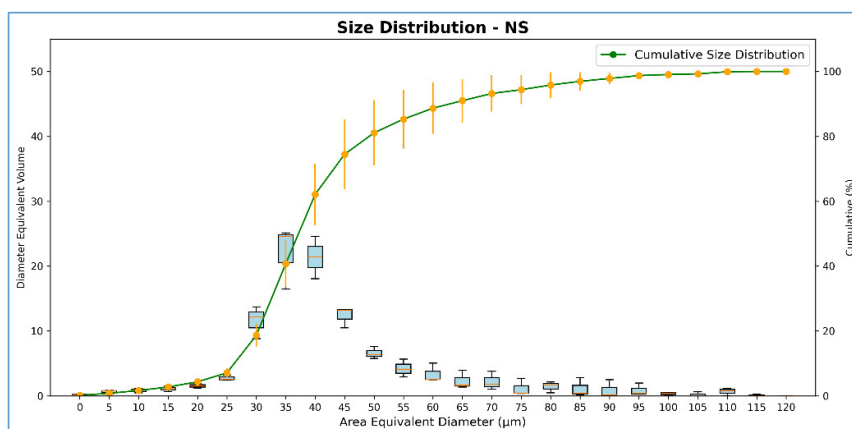


Figure 2.7: Diameter size distribution for gas atomized powder (NS)

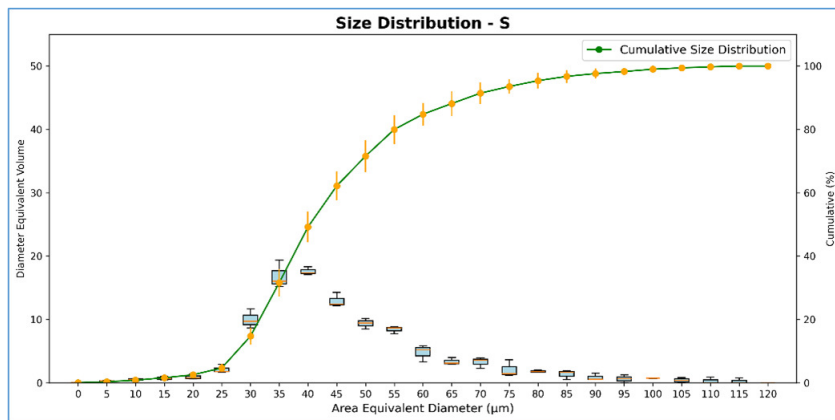


Figure 2.8: Diameter size distribution for spheroidized powder (S)

2.6.2 | Particle shape

The shape of particles is characterized by their form (overall shape), roundness (large-scale smoothness/angularity), and surface texture (small-scale smoothness/roughness). The shape factor dimensionless quantities used in image analysis and microscopy that numerically describe the shape of a particle. The most commonly used factors are:

- Aspect Ratio is defined as the ratio of the Feret's minimum length to the Feret's maximum length, always falling within the range $0 < AR \leq 1$ and expressed as a dimensionless value.
- Circularity measures the degree to which the projection of a particle resembles a circle, considering both the particle's form and the smoothness of its perimeter.

The circularity analysis conducted on NS and S powders revealed distinctive characteristics in their particle shapes and uniformity (Figure 2.9 and Figure 2.10). In the case of NS powder, circularity values spanned from 40% to 100%, reflecting a diverse range of particle shapes and sizes. Notably, over 50% of the NS powder particles exhibited circularity values surpassing 90%, indicating a substantial proportion of particles with high circularity. While the S powder exhibited a narrower circularity range of 50% to 100%, with more than 95% of its particles achieving circularity values exceeding 90%. This suggests a higher prevalence of nearly spherical or highly regular-shaped particles within the S powder sample. Furthermore, the analysis revealed a lower spreading of box plots and smaller error bars for the S powder, indicating a higher degree of uniformity in particle shapes compared to the NS powder.

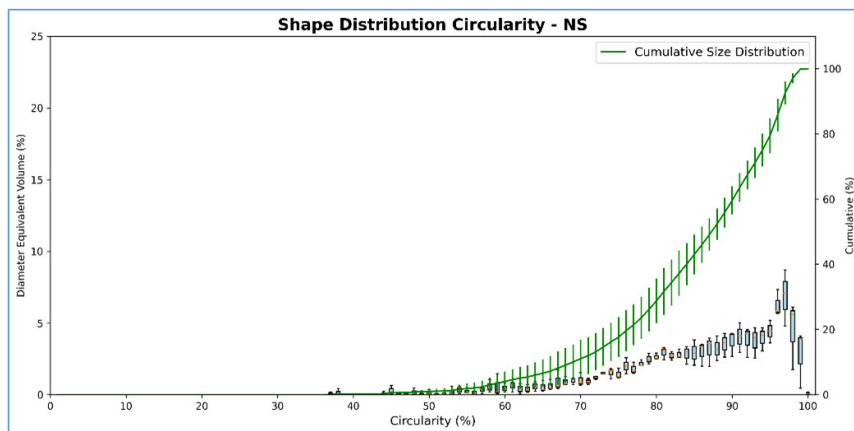


Figure 2.9: Shape distributions for gas atomized powder (NS)

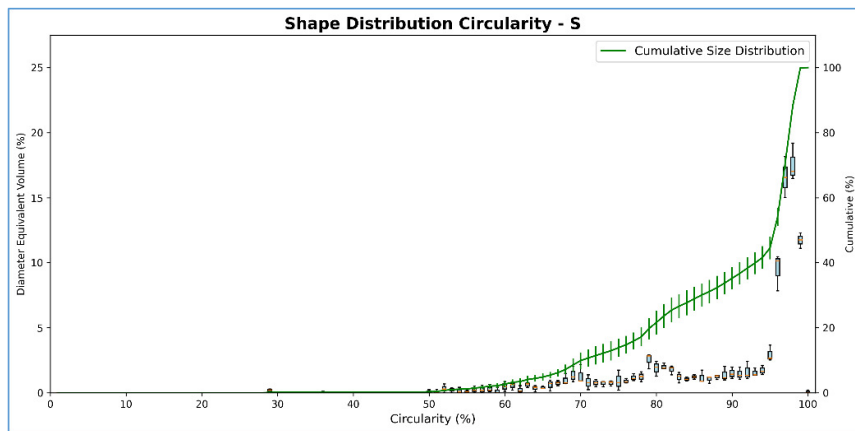


Figure 2.10: Shape distributions for spheroidized powder (S)

2.7 | Material Characterization

2.7.1 | Identification of the powder type

The SEM examination of two powder samples, one subjected to spheroidization and the other non-spheroidized, observations were made at 500x magnification using both BSE and SE imaging. Notably, the non-spheroidized powder (Figure 2.11) exhibited a higher prevalence of small satellite particles surrounding larger powder particles. The discernible presence of small satellite particles around larger ones in the non-spheroidized powder provides a clear visual indicator distinguishing it from the spheroidized (Figure 2.12) counterpart. This visual evidence establishes a reliable method for identifying whether a powder has undergone spheroidization, contributing valuable insights into the morphological characteristics of the examined samples.

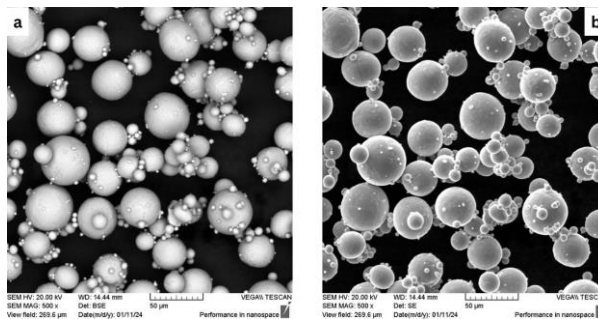


Figure 2.11: Microscopic view of powder sample NS a) BSE b) SE

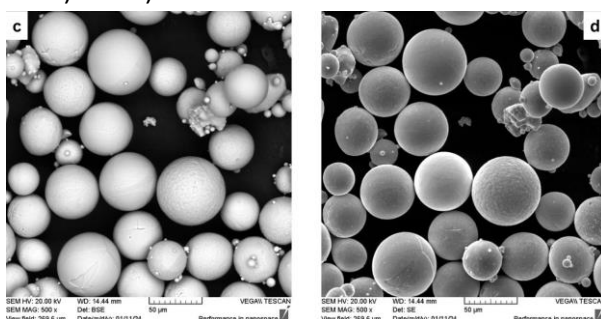


Figure 2.12: Microscopic view of powder sample S c) BSE d) SE

2.7.2 | Chemical composition

- Non-Spheroidized (NS)

The SEM analysis of the powder in two distinct zones reveals nuanced variations in elemental composition. In Zone 9, there is a marginal reduction in Titanium content, suggesting a localized difference in the powder's composition. Conversely, Aluminium and Vanadium exhibit slight increases in Zone 9 compared to Zone 8. The absolute errors associated with the measurements are minimal, affirming the reliability and precision of the analytical technique. The Netto values, representing net intensities, indicate disparities in element concentrations between the zones, with higher values signifying a more pronounced presence of specific elements.

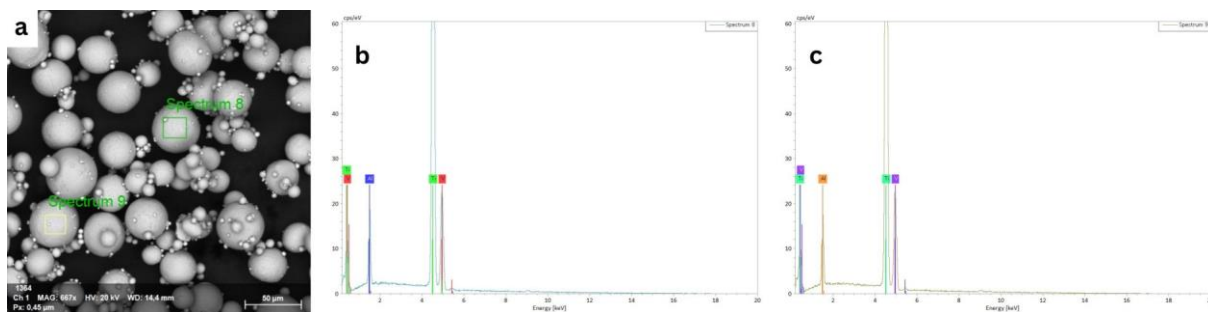


Figure 2.13: (a) Identification of zones (b) Material Characterization graph zone 8 (c) Material characterization graph zone 9

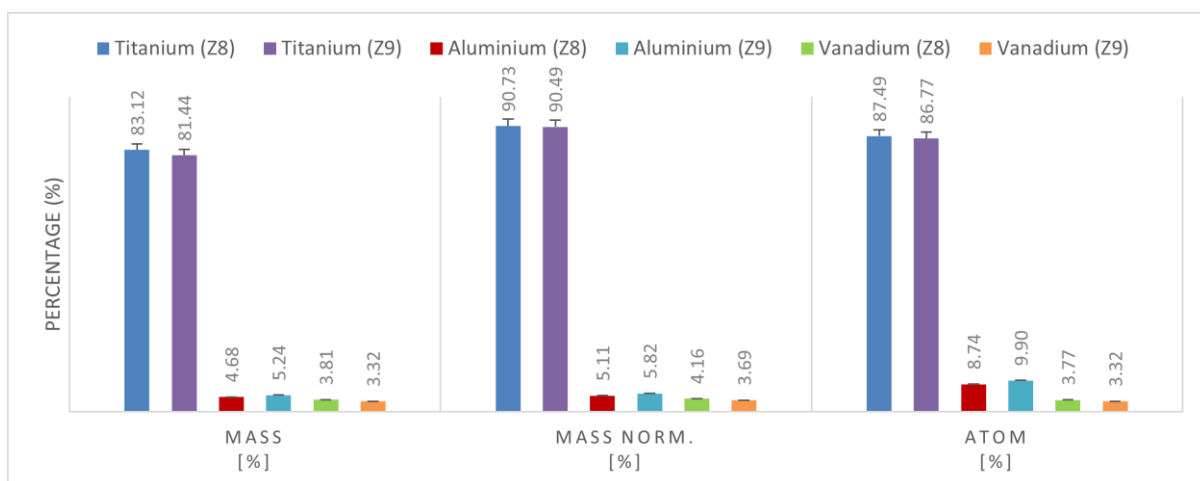


Figure 2.14: Material Characteristic data comparison between Zone 8 and Zone 9

Table 2.3: Chemical composition parameters (NS)

Element	Atomic No.	Netto	Mass (%)	Mass Normal (%)	Atom (%)	Abs error (%) (1σ)	Rel. error (%) (1σ)
Titanium (Z8)	22	135150	83.12	90.73	87.49	2.34	2.81
Aluminum (Z8)	13	9506	4.68	5.11	8.74	0.26	5.64
Vanadium (Z8)	23	5776	3.81	4.16	3.77	0.19	4.96
Titanium (Z9)	22	137800	81.44	90.49	86.77	2.29	2.81
Aluminum (Z9)	13	9131	5.24	5.82	9.90	0.29	5.59
Vanadium (Z9)	23	5186	3.32	3.69	3.32	0.18	5.34

- Spheroidized

Continuing from the previous experiments, the SEM analysis of the powder in two additional zones sheds further light on its chemical composition. In Zone 11, similar trends to Zone 9 are observed, with a marginal reduction in Titanium content and slight fluctuations in Aluminum and Vanadium mass percentages compared to Zone 10. The absolute errors associated with the measurements remain consistently low across all zones, indicating reliable and precise data collection. Netto values continue to reveal variations in element concentrations between the zones, reaffirming the heterogeneous nature of the powder.

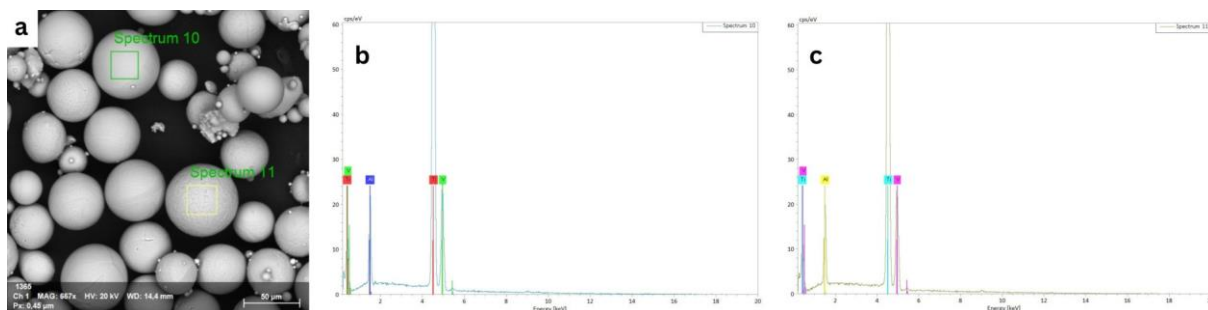


Figure 2.15: (a) Identification of zones, (b) Material Characterization graph zone 10, (c) Material characterization graph zone 11

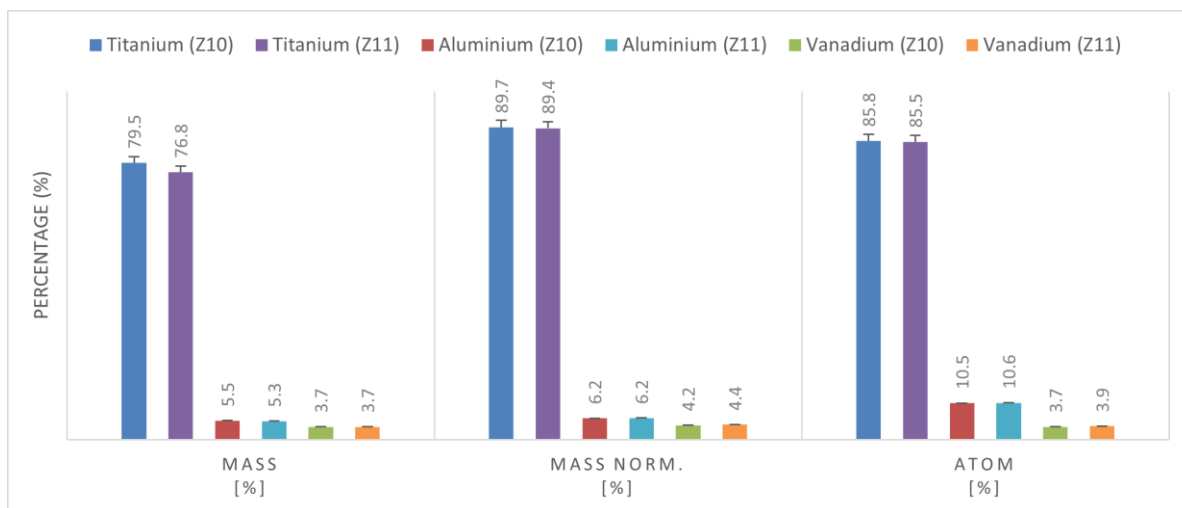


Figure 2.16: Material Characteristic data comparison between Zone 10 and Zone 11

Table 2.4: Chemical composition parameters (S)

Element	Atomic No.	Netto	Mass (%)	Mass Normal (%)	Atom (%)	Abs error (%) ($\pm 1\sigma$)	Rel. error (%) ($\pm 1\sigma$)
Titanium (Z10)	22	132057	79.5	89.7	85.8	2.24	2.82
Aluminum (Z10)	13	11114	5.5	6.2	10.5	0.30	5.51
Vanadium (Z10)	23	5866	3.7	4.2	3.7	0.18	4.94
Titanium (Z11)	22	133182	76.8	89.4	85.5	2.16	2.82
Aluminum (Z11)	13	10317	5.3	6.2	10.6	0.30	5.55
Vanadium (Z11)	23	5984	3.7	4.4	3.9	0.18	4.89

The combination of SEM analysis and quantitative data reaffirms the nuanced variations in the chemical composition of the powder. These findings provide valuable insights into the elemental distribution and characteristics of the material, further enriching our understanding of its properties and potential applications.



2.8 | Conclusions

- In powder characterization literature, in which the gas atomization and the plasma spheroidization processes are compared, plasma spheroidization produces generally smaller powder particles, as well as more rounded ones; opposed to gas atomization which provides bigger particles with some satellites. However, when examining the results for the densities as well as flowability, in literature, both powders have quite similar results for flowability and densities, with plasma spheroidization having slightly lower flowability time and higher apparent density than gas atomization.
- We observed a difference between NS and S powders. With the spheroidized powder obtaining better results in terms of flowability and tap density. This can be due to its reduced surface area, uniform shape, better packing efficiency, less segregation and better dispersion of the particles. This causes spheroidized powder to have better manufacturing efficiency, higher product quality and enhanced cost-effectiveness.
- The comparison between NS and S powders highlights their contrasting particle size distributions and shape uniformity, emphasizing the distinct influence of the spheroidization process on enhancing particle geometries. Spheroidization demonstrates an excellent capability in improving particle shapes, particularly evident in the enhanced uniformity and regularity observed in S powder compared to NS powder, as seen in powder morphology distributions and the narrower circularity ranges with smaller errors in the S powder analysis. These findings underscore the advantages of spheroidized particles in achieving consistent and predictable powder properties for diverse applications.
- The distinction between spheroidized and non-spheroidized powder was discerned through SEM analysis, where the presence of numerous small satellite particles surrounding larger particles was observed. Additionally, the nuanced variations in chemical composition between different zones of the powders, with variations observed in Titanium, Aluminum, and Vanadium content. Absolute errors associated with the measurements were consistently low, indicating reliable data collection.



3 | Laser Cladding

Authors: Mennatalla Gad, Reality Amoh, Folco Perego, Wiseman Siriro, Soukaina Tachfouti

3.1 | Introduction

In the field of additive manufacturing, deposition methods vary widely based on material characteristics and application requirements. This section offers some insight into laser cladding (LC) and compares an LC deposit with a cold spray (CS) coating. LC finds extensive application in diverse industrial sectors, including rapid manufacturing, parts restoration, surface coating, and the advancement of novel alloys. Its versatility lies in the ability to combine diverse powder types and control the feed rate of powder flow, facilitating the production of heterogeneous components. LC enables the creation of coating typically ranging from 50 µm to 2 mm, forming a homogeneous deposit through fusion on top of the substrate[7]. On the other hand, CS presents a different adhesion mechanism characterized by the utilization of metal powders propelled by a supersonic gas jet for coating deposition. The micro-structure of the bulk powder is preserved in cold spray coatings, except at particle boundaries. At these boundaries the extreme shear rates cause grain refinement and nanograin formation to take place, leading to a high degree of particle-to-particle bonding. This yields a coating with tensile strength comparable to the annealed material, albeit with a noticeable reduction in ductility and an increase in hardness. Key attributes of CS encompass compressive residual stresses, elevated strength, and minimal heat input to the substrate. Typically, this technique is employed for joining hard to weld materials.

3.2 | Objectives

The aim of this section is to optimize the laser cladding parameters and compare the results with a cold spray deposit of the same powder. Among the variety of parameters affecting laser cladding the two single out by this report are: powder feed rate and track overlap. Thus the objectives include:

- 1) Finding the optimal feed rate for a height to width ratio of 0.2 of the clad track.
- 2) Examining the effect of different overlapping coefficients.
- 3) Analyzing the microstructure of the LC deposit with a cold spray deposit.

3.3 | Material and Parameters

The substrate material is a Special Alloy Steel: 42CrMo4 (42CD4) with medium carbon content.

Fe	C	Si	Mn	P	S	Cr	Mo
wt% 96.8 – 97.8	0.38-0.45	0.40	0.60-0.90	0.025	0.035	0.90-1.20	0.15-0.30

Table 3.1: 42CD4 substrate composition[8]

The powder material is plasma transfer arc (PTA) SS316 austenitic steel with the following composition:

Fe	Ni	C	Si	Mn	P	S	Cr	Mo
wt% 61.9 - 72	10 - 14	0.07	0.75	2.0	0.045	0.030	0.90-1.20	2.00-3.00

Table 3.2: SS316L powder composition[9]

The CS substrate material is a 6000 series Aluminium.

3.3.1 | Process Parameters

In laser cladding, a feeder system feeds powder into a laser-generated melt pool by a stream of inert gas passing via a nozzle (Fig.3.1). The powder feeding system must be capable of providing the appropriate amount of powder to the laser contact zone. In the considered configuration, the powder is delivered by a gravity feeder system with a light gas flow (5L/min). The procedure begins with a laser beam that irradiates a tiny layer of substrate, resulting in a melt pool. Powder is then pumped into the cladding zone and melted. Subsequently, the laser-powder delivery system continues its path: the melt pool begins to solidify and clad begins to form. The condition that determines whether the delivered powder adheres to the cladding zone to form the clad or not is defined by the type of impact.

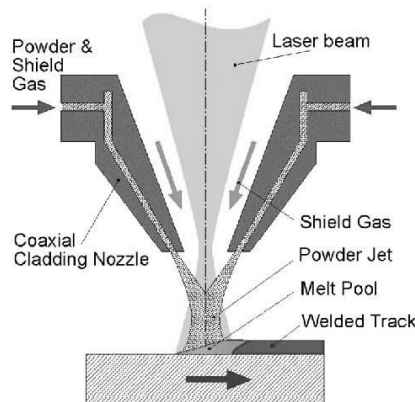


Figure 3.1: Coaxial laser cladding deposition schematic[10]

The main phenomena involved in LC are:

- Absorption
- Conduction
- Diffusion
- Solidification

The fixed parameters for the current laser cladding set up include:

Parameter	Value	Units
Operating distance	13	mm
Laser power	3	kW
Speed	1	m/min

Table 3.3: Laser cladding parameters

The laser source was a fiber diode laser. The cladding head employed is a PRECITEC Copper nozzle with cooling system keeping 15°C. The powder is fed dynamically into the melt pool formed by the laser source at a rate ranging from 30 to 60g/min. The simultaneous movement of the laser source and feeding system results in a coating with a track width of 4 mm.

3.3.2 | Clad beam geometry

Research shows the optimal height to width ratio to be around 0.2[11]. Fig.3.2 shows the key geometric features of a bead cross-section: H: clad height, thickness of the bead above the surface of substrate W: width of the bead Ac: clad area Am: molten area

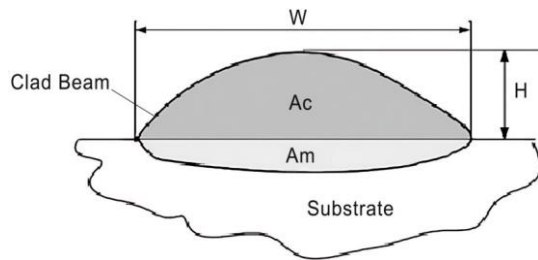


Figure 3.2: Clad beam cross-section [12]

For width W:4mm, the height of the cladding has been defined between H:0.7-0.8mm And for W:6mm, H:0.1-1.0 mm

3.4 | Coating characterization

3.4.1 | OM Sample preparation

Optical microscopy (OM) was used for the characterization of the material microstructures. The samples were created by embedding the test specimens ($\sim 1 \text{ cm}^2$) in ceramic resin using the compression hot mounting machine SimpliMet 400. Polishing with abrasive papers (grit progression: 250, 600, and 1200) and lapping with diamond particles (9 and $3\mu\text{m}$) and SiC particles ($0.05 \mu\text{m}$) were applied to obtain a mirror-like surface. The chemical etching was carried out using Aqua Regia.

3.4.2 | Hardness testing

The Vickers hardness tests have been carried out on the 5-layer samples of the LC deposit, with loads 300g with 20 indentations in a straight line. The distance between each indentation was of 0.1 mm for a total distance of 1.9mm. For the CS the test was limited to random sampling on the substrate with a 200g load.

3.4.3 | SEM imaging

Operating in high vacuum atmosphere, the SEM has been used for the observation of the microstructural details and to study material dilution. BSE X-ray spectroscopy was combined with the spatial resolution of the electron microscope to obtain energy dispersive spectroscopy (SEM-EDS) mapping to observe the material distribution.

3.5 | Results and Discussion

The 42CD4 substrate's diameter measured 45.2 mm. The desired clad height to width ratio is 0.2, and the approximate track width is 4mm. Thus, the aim is to obtain a uniform deposit thickness of around 0.8mm by tuning the feed rate and overlapping coefficient.

3.5.1 | Optimal feed rate identification

To find the optimal feed rate and overlapping, experiments were replicated with 4 single track clads (Fig.3.3a) 4 times over a range of values. The initial feed rate was set at 7.5 rpm with the 4 tracks progressing up to 11.5 rpm. The table below summarizes the findings.

Track #	Feed rate (rpm)	Diameter (mm)			
		Group 1	Group 2	Group 3	Group 4
1	7.5	46.4			
2	8.5	46.7	46.6	46.6	45.7
3	9.5	47	47	46.9	45.9
4	10.5	47.2	47.3	47.2	46.3
4	11.5		47.6	47.4	

Table 3.4: Feed rate effect on deposit size

The data in the Fig.3.3b reveals a positive correlation between feed rate and deposit thickness, suggesting that higher feed rates result in thicker deposit layers. As the feed rate increases from 7.5 rpm to 11.5 rpm, there is a corresponding increase in the diameter of the deposit, from which the track height was calculated. Specifically, the diameter seems to grow linearly from a min. of 46.6mm to a max. of 47.6mm, with relatively low scatter for a process with such complexity and variability such as LC. The optimal feed selected was 8.5 rpm.

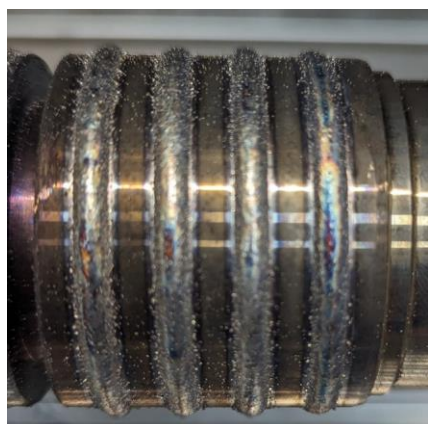
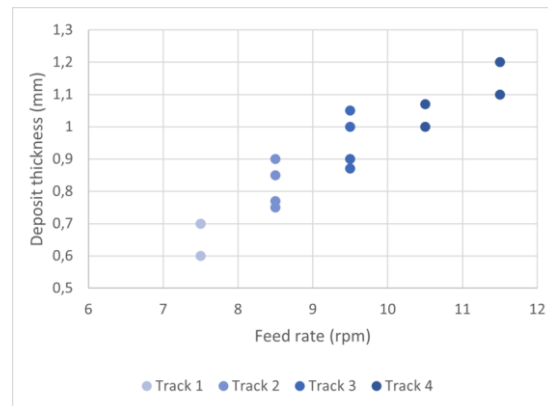

(a) Single clad tracks

(b) Clad thickness for increasing feed rate

Figure 3.3: Feed rate analysis

3.5.2 | Optimal overlap identification

Keeping a constant feed rate of 8.5 rpm, 3 new tracks with increasing overlap were deposited over a total length of 16 mm.

Track overlap (%)	Diameter (mm)			
	Group 1	Group 2	Group 3	Group 4
30	45.8	46.9	46.8	46.8
40	46	47.1	47.0	
50		47.4	47.4	
70				47.9

Table 3.5: Overlap effect on deposit size

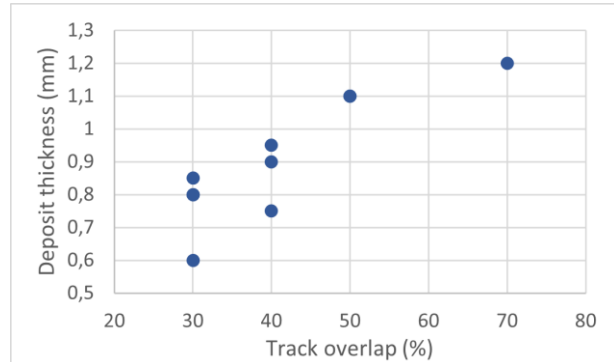
(a) 30% 50% 70% overlap

(b) Clad thickness for increasing feed rate

Figure 3.4: Overlap analysis

Based on the data provided above, it appears that an increase in track overlap from 30% to 70% corresponds in an overall increase in the diameter of the deposition track and thus the thickness of the deposited material. The thickness is not uniform but displays pronounced peaks and valleys. The surface flatness of the coating can be thus considered a function of the overlapping distance, which will significantly affects its quality and machining allowance for subsequent processing[13]. It must be noted that an excessive material overlap can potentially increases the risk of defects[14]. The overlap coefficient was thus forward set to 30%.

3.5.3 | Temperature effect on the substrate

After performing a 5 layer deposition over a 50 mm length with feed rate 8.5 rpm, 30% overlap, speed, 1m/min and laser power 3kW, a significant temperature increase was noticed. A color change of the substrate is the effect of the oxidation. This might be due to the size of the specimen. Smaller specimens can influence the process results given their sharper temperature change rate and higher overall temperature, even reaching up to 900°C and staying hot for several hours. This temperature can produce undesirable effects on the substrate. A closed loop control feedback with thermal sensor for continuous monitoring could help circumvent the issue. The final coating diameter measured 53.3mm, the total coating 4.05mm with each each layer deposited about 0.81mm thick.

3.5.4 | Optical microscopy

Optical microscopy (OM) analysis was conducted on the 5 layer laser cladded samples to examine their geometric dilution and HAZ size. Analyses were done at different magnifications: 2.5x, 5x, 10x and 20x. For this single-track sample, the feed rate was 11.5 rpm, speed 1m/min and laser power 3kW. Fig.3.5 illustrates a reconstruction of an entire clad cross-section with a clad height measured to be around 1 mm, which is consistent with the physical measurement.

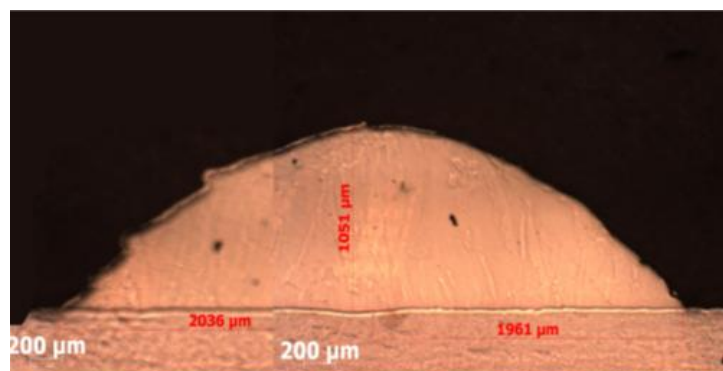
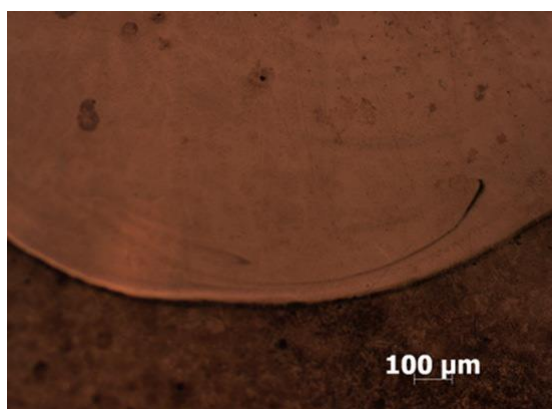
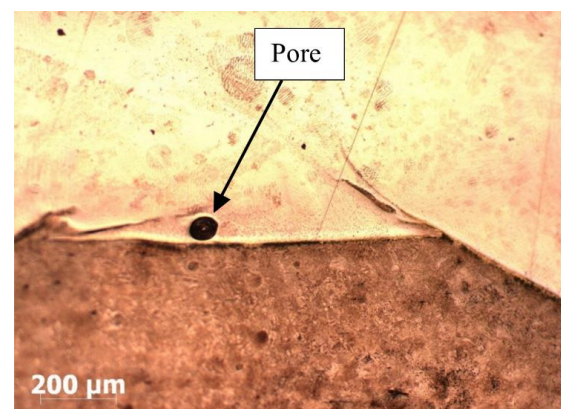


Figure 3.5: Single track optical microscopy reconstruction



(a) OM 20x magnification



(b) OM 5x magnification

Figure 3.6: SS316L powder geometric dilution in the substrate

The tracks exhibit a boundary layer of good dilution and adhesion between the two materials with minor porosity. Fig.3.6 show the boundary layer between the deposit and the base material. No grains were observed, which might be due to the over etching of the sample. Additionally, some scratches and defects were identified in the sample under higher magnification. Some defects were observed in the sample as shown in Fig.3.6b. Porosity in the material could be attributed to inadequate remelting of the adjacent clad track or insufficient protection of the molten pool from atmospheric gases. This can result in gas contamination and porosity in the deposited material. Another probable reason for porosity is the presence of surface contaminants and oxides. Unfortunately such impurities can easily become entrapped inside the material in high temperature processes. Fig.3.7 shows the different layers at the interface between deposit and substrate. The heat affected zone (HAZ) measured $\sim 0.5\text{mm}$ for all samples. This relatively small fusion zones indicates that the process parameters were properly optimized. The HAZ is inevitable in LC due to the melting of the material and the subsequent heat dissipation. However, it is recommended to minimize the HAZ as much as possible to avoid compromising the surface mechanical properties such as fatigue resistance, distortion, and making it prone to surface cracking. Furthermore, the substrate material exhibits fine columnar grains near the HAZ, transitioning towards equiaxed grains as we go deeper into the material. This phenomenon hints at a progressive change in the material properties and composition in the fusion zone as the heat penetrating the substrate creates a temperature gradient. This gradient influences the recrystallization time of the substrate.

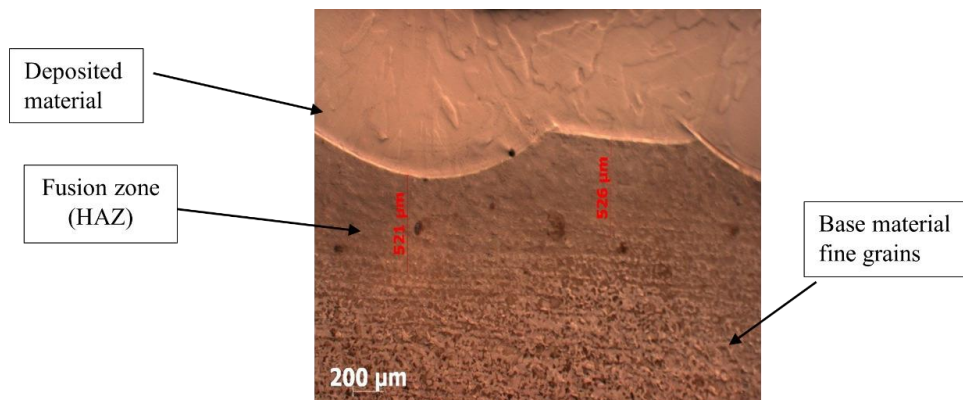


Figure 3.7: 316L on 42CD4 HAZ penetration

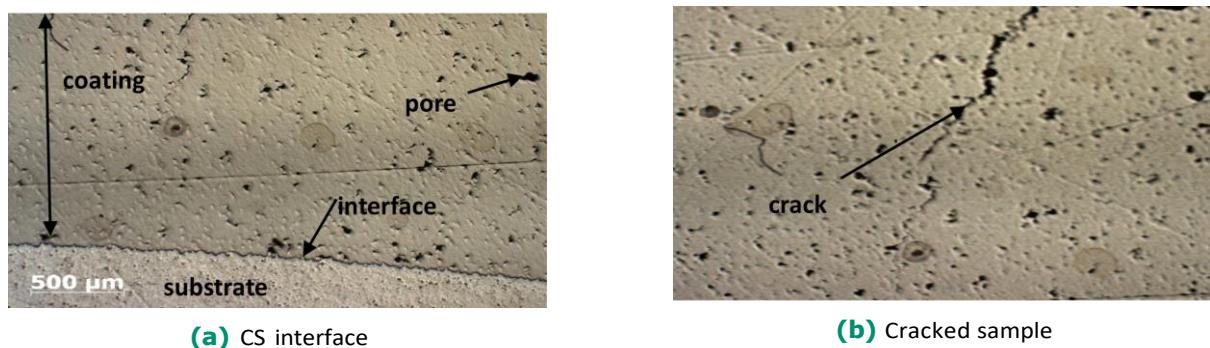


Figure 3.8: Cold spray (CS) optical microscopy observations

The comparison with a cold spray deposit highlights several key differences. The pore shown in Fig.3.8a above is likely due to a poorly adhered particle, dislodged during the cutting and polishing of the sample. This is not the same as in laser cladding where the bonding of particles is better. Numerous cracks were observed such as the one in Fig.3.8b. This imperfections are a consequence of the low ductility of the deposited material. When a machining operation was later on conducted on the cold sprayed sample, the process was unsuccessful, due to these defects. It is therefore necessary to perform a heat treatment on a cold-sprayed sample to increase ductility and strength and improve its machinability.

3.5.5 | SEM Imaging and Analysis

Fig. 3.9 show the SEM imaging of laser cladding and cold spray samples respectively. Observing the two interfaces the bonding mechanism of the two processes appears quite different. For the laser cladding (Fig. 3.9a), there is grain recrystallization, whereas on the cold spray sample (Fig. 3.9b), the impact of the steel particles on the softer aluminum substrate on the caused deformation with some particles trapped into the substrate. In the case of laser cladding with overlapping tracks of 30% at 8.5 rev/min, the chemical dilution obtained is the range of 10 to 20 μm . This level of dilution is not excessive and guarantees a good metallurgical bonding between the clad and the substrate without compromising the material properties or the performance of the coating.

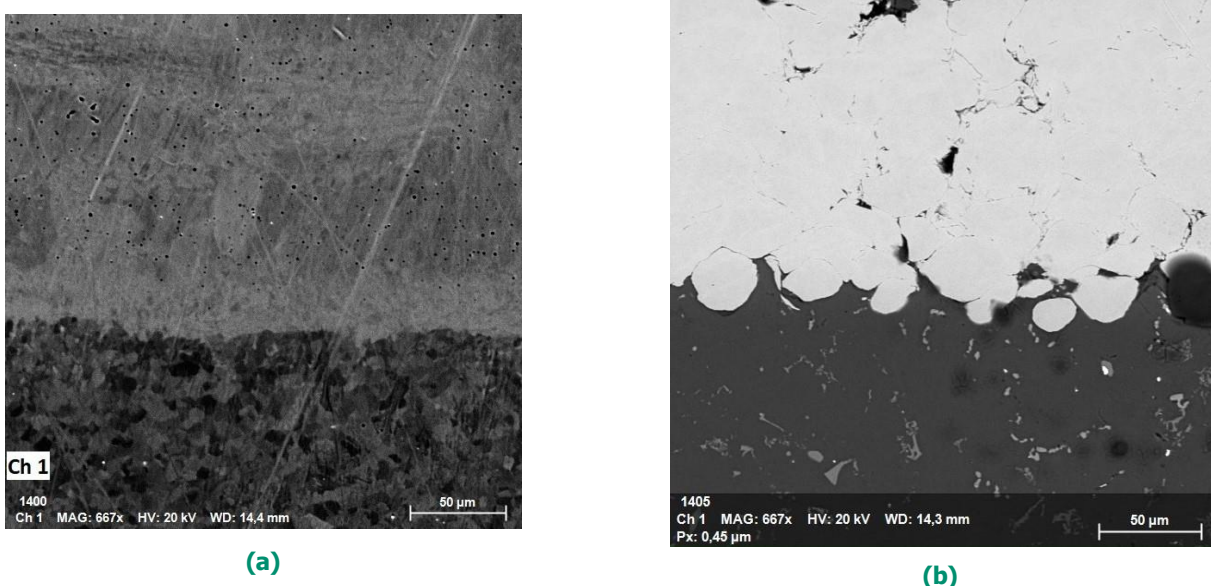


Figure 3.9: LC (a) and CS (b) BSE SEM imaging

The elemental mapping in Fig. 3.10 shows the material distribution at the interface between the coating and substrate. The minimal thermal input of the CS process is evidenced by the complete lack of any of the 316L elements in the substrate (Fig. 3.10b), with the exception of the mechanically entrapped particles. Fig. 3.10a shows the chemical dilution of the two materials due to fusion.

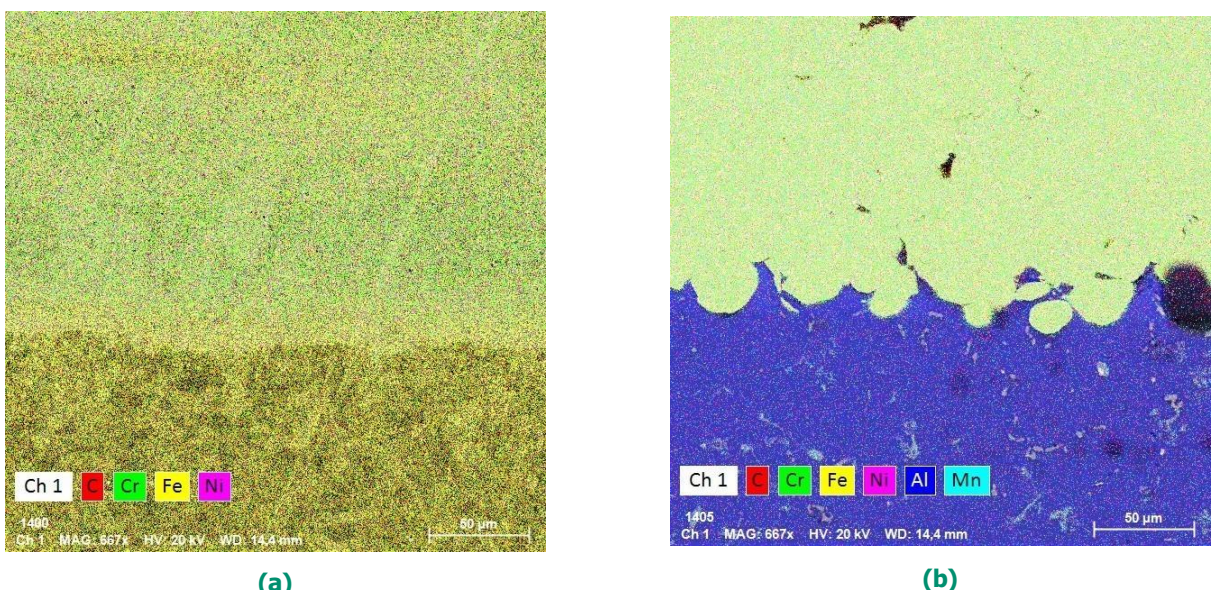


Figure 3.10: LC (a) and CS (b) elemental mapping

3.5.6 | Microhardness testing

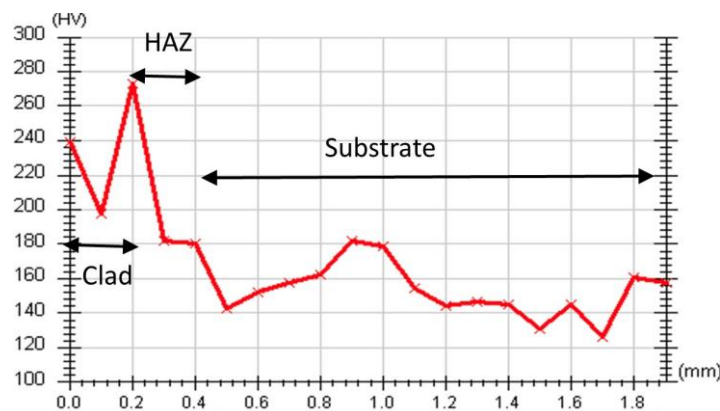


Figure 3.11: Microhardness variation along clad deposit and substrate

The average hardness value of the substrate is around 160 HV, whereas the average hardness value of the clad zone is around 240 HV. Compared with the original material, the hardness of the clad layer obtained by laser cladding is greatly improved, i.e. from around 152 HV to around 240HV. The quick solidification process occurring during laser cladding induce a recrystallization of finer grains. This fine and dense grains result in a noticeable higher hardness of the clad layer. Peak hardness was generally observed at 0,2mm and that is the heat-affected zone (HAZ). It is harder than the substrate and the coating, with a hardness value of about 260 HV. The reason for this is that the HAZ undergoes a thermal cycle of rapid heating and cooling, resulting in a zone that is harder than the coating and the substrate. The values in Table 3.6 are sampled at random spots on the cold spray deposit. Thus, the large data

Measure	Load (g)	Hardness (HV)
1	200	350.1
2	200	354.5
3	200	306.5
4	200	259.7
5	200	192.1

Table 3.6: CS sample micro hardness

spread may be attributed to the effects discussed during the microscopic evaluation (Sec.3.5.4), such as the difference in particle adherence and cracking. Despite the different loads, the two data set can be compared since within this load range, Vickers hardness values are generally independent of the test force. It can therefore be deduced that 316L Stainless Steel cold sprayed microhardness values are higher than the LC ones, with an 100% increase in hardness: from 152 HV to 350 HV. The ability of cold spray to produce coatings with almost double hardness is a result of the deformations happening due to the high impact speeds of the particles into the substrate. Beyond the strain hardening, an additional factor contributing to the hardness increase is grain refinement due to severe plastic deformation, as was noticed from microstructure observation that the deposit is characterized by a smaller grain size. The higher number of grain boundaries act as an obstacles for dislocation movement.

3.6 | Conclusions

In the present study, the deposition of 316L Stainless Steel powder has been carried out by direct laser cladding using a continuous-wave diode laser with an optimum power of 3000 W, on an AISI 4140 Alloy Steel rod with a diameter of 45.3 mm. This was then compared to a cold spray deposition of the same powder on a 6000 series aluminum substrate. The yielded results are the following:

- Exploring optimal overlap revealed the direct correlation between overlap percentage, substrate diameter, and deposit thickness. After experimenting with different powder feed rates and overlapping percentages, it was concluded that the best homogeneity of the coating material on the substrate



occurs at an overlapping percentage of 30% with 8.5 rev/min. While higher overlaps enhanced material deposition, thermal effects on the substrate integrity were noticed. The high thickness of deposited coats impacts the thermal properties of both the coat and the substrate greatly, especially the HAZ. On average, the 5-layer deposit yielded the expected coating thickness of 0.81 mm.

- Optical microscopy and SEM analysis provided valuable insights into microstructural characteristics. The SEM snapshots taken at different magnifications show that there is a dilution area of approximately 10 µm between the coating and the substrate. This zone also changed the chemical composition, particularly in the iron element. In general, the examined coated samples showed no cracks or pores. The samples have good metallurgical contact with a small dilution zone.
- The microhardness results indicate that the LC coating layer exhibits higher hardness properties than the substrate.

3.6.1 | Cold Spray comparison

- In the cold spray analysis, 316L Stainless Steel was sprayed over an aluminum rod. The results revealed the unique properties of cold-sprayed coatings, with no HAZ or chemical dilution and improved hardness due to the extreme deformation of the powder.
- Despite some observations of porosity and compromised integrity, there's significant enhancement in material properties, as indicated by microhardness testing.
- Heat treatment could increase ductility and strength, thus improving machinability.

In summary, this practical experiment not only deepened our understanding of laser cladding and cold spray processes but also highlighted the importance of parameter optimization for achieving consistent and high-quality mechanical and metallurgical properties for different applications in advanced manufacturing.

4 | Belt Finishing

Authors: Duressa Guta Asrat, Md Ibthisum Alam, Pervez Alam Khan, S M Faysal Ahmed, Mengstie Endale Getu

4.1 | Introduction

Belt finishing is a precision manufacturing process, which utilizes abrasive belts to produce mirror polished metallic surface with a very low surface roughness and induced compressive residual stress [15]. Among many applications, automotive and aerospace sectors are particularly focusing on manufacturing functional smooth surface components to enhance precision, performance, and reliability. Belt finishing process combined with hard turning process has shown impressive results to meet this requirement. Besides, this process is gaining increasing attraction from the industry thanks to its minimal investment requirements and ease of handling [16] . The underlying mechanism of the belt finishing process can be explained with figure 4.1 below.

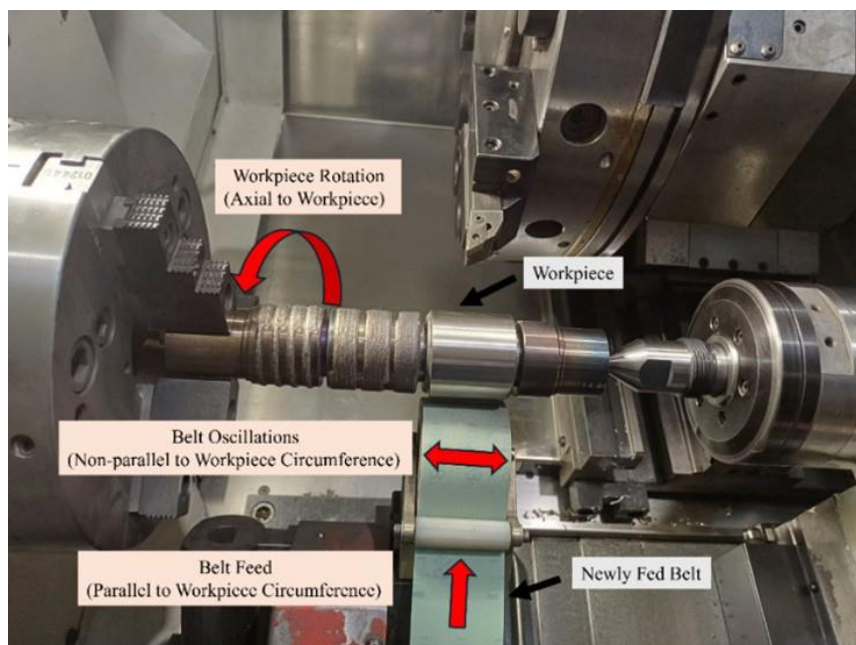


Figure 4.1: Belt finishing process

The primary components of this process are the belt and the workpiece. Generally, the belt contains a single layer abrasive grain, applied against a rotating workpiece on the setup. The hard turned surface of the workpiece undergoes circumferential scratching by the belt, resulting in a reduction of its roughness. The belt is provided with a low feed rate to facilitate a consistent contact between the belt and the workpiece. Throughout the process, the worn belt does not reappear as the new abrasives replace them simultaneously. In addition to the circumferential feed, the belt is exerted to oscillate in the axial direction of the workpiece. This oscillation results in an added non-circumferential scratching of the workpiece, improving the utility of the process [16][17].

4.1.1 | Factors Influencing the Belt Finishing Process

- (i) **Belt Grain Size:** The belt grain size typically ranges from 0 to 100 μm . The suitable grain size depends on the quality of hard turned surface and intended application. The selection of grain size has a significant impact on the final surface roughness [18].
- (ii) **Lubrication Condition:** Belt-finished can be performed under three lubrication conditions such as dry, lubricated or MQL (Minimum Quantity Lubrication). Studies have suggested the potential of MQL in diminishing the surface roughness.
- (iii) **Operating Parameters:** Belt feed rate, belt oscillation frequency, workpiece rotating speed and



contact area during the operation need to remain in the optimal range for generating expected workability. Besides, belt finishing time with certain belt grain size is also an important criterion to minimize the power usage.

4.1.2 | Evaluation of Surface Roughness Measurement Parameters

Belt finishing profoundly enhances the surface integrity by improving the microstructure, generating compressive residual stresses and reducing the surface roughness. The integration of belt finishing does not only keep the Ra (Average Roughness) value below $0.1 \mu\text{m}$ but also ensures a homogenous surface across the entire workpiece [19]. In terms of expressing surface roughness, the most common parameters in practice are:

- **Ra (Average Roughness):** The arithmetic average of the absolute values of the roughness profile deviations from the mean line within the evaluation length.
- **Rz (Total Roughness):** The total height difference between the highest peak and the lowest valley within a specified length.

However, in accurately characterizing functional surfaces following superfinishing processes, there are instances where these parameters may not accurately portray the actual surface texture. On this context, the Abbott-Firestone curve or bearing area curve (BAC) parameters can prove to be useful.

- **Rpk (Reduced Peak Height):** The average height of the peaks within the evaluation length. It indicates the peaks which will be removed during the first phase of the contact.
- **Rk (Core Roughness Depth):** The average depth of the valleys within the evaluation length. This parameter indicates the level at which the surface will be modified.
- **Rvk (Reduced Valley Depth):** The average depth of the valleys within the evaluation length without any leveling process. It is indicated as the lubrication criterion for the oil retention.

4.2 | Objectives

The main objective is to predict the final roughness for turned surface using belt finishing process by controlling process parameter on laser cladded work material SS316L. Also, to observe the effect of belt finishing process on the turned surface under two different belt abrasive grit size and determine required time to get the signature of each grit size.

4.3 | Materials and Methods

4.3.1 | Material and Equipment

A TRANSMAB T450, 3-axis turning machine, is utilized in the workshop for turning and belt finishing operation. Belt of abrasive material alumina (Al_2O_3) with two different grits: 80 for aggressive initial leveling, removing substantial irregularities, and 40 for subsequent fine polishing, achieving an exceptional final surface finish is used for belt finishing.

The workpiece employed in this study consists of SS 316L material, which has been deposited onto low carbon steel through the process of laser cladding. The procedures for this study are then applied on the workpiece as indicated in sections 4.3.2; 4.3.3; 4.3.4 below. Contact profilometer was utilized to measure and assess the surface quality of the completed item.

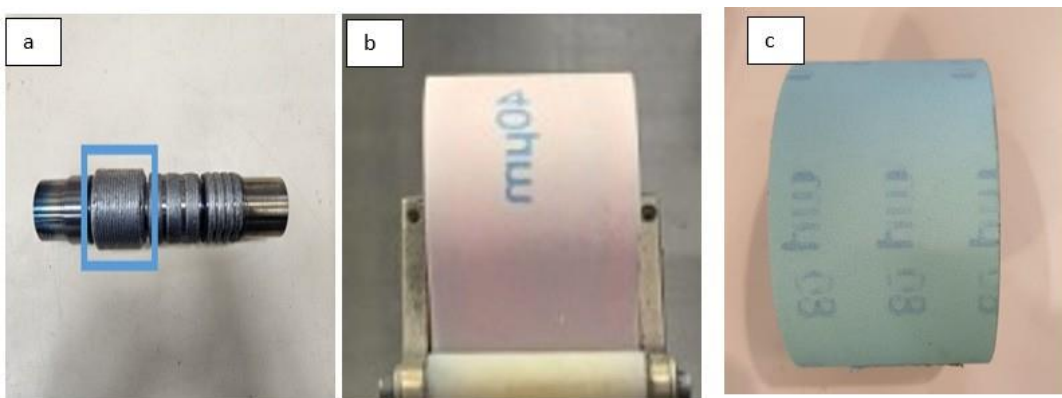


Figure 4.2: (a) Laser cladded work material, (b) 40-micron belt and (c) 80-micron belt

4.3.2 | Turning

Within the context of this workshop, the CNC lathe machine is essential to accurately and effectively performing the turning process. The turning operation is performed on a CNC machine TRANSMAB T450 3 axis turning machine under dry condition. The turning process is performed under the parameters given in Table 4.1 below.

Table 4.1: Turning parameters.

Parameters	Values	Units
Depth of cut	0.5	mm
Feed	0.2	mm/rev
Cutting speed	120	m/min

4.3.3 | Belt Finishing

The belt, which has two different abrasive grain sizes, is used to provide the turned portion to enhance surface roughness of work material. By using belts with varying grain sizes, the material removal process was carefully controlled to achieve the required surface properties. The belt finishing operation is performed under the conditions in the table below with varying process time at constant tangential speed and dry condition.

Table 4.2: Belt finishing conditions.

Belt finishing parameters	Values	Units
Alumina abrasive Grain size	80 and 40	µm
Pressure	5	Bar
Belt feed rate	100	mm/min
Work material rotation speed	120	m/min
Duration of time per operation	10	s
Initial roughness (Ra) work material	2.008	µm
Cutting speed	120	m/min

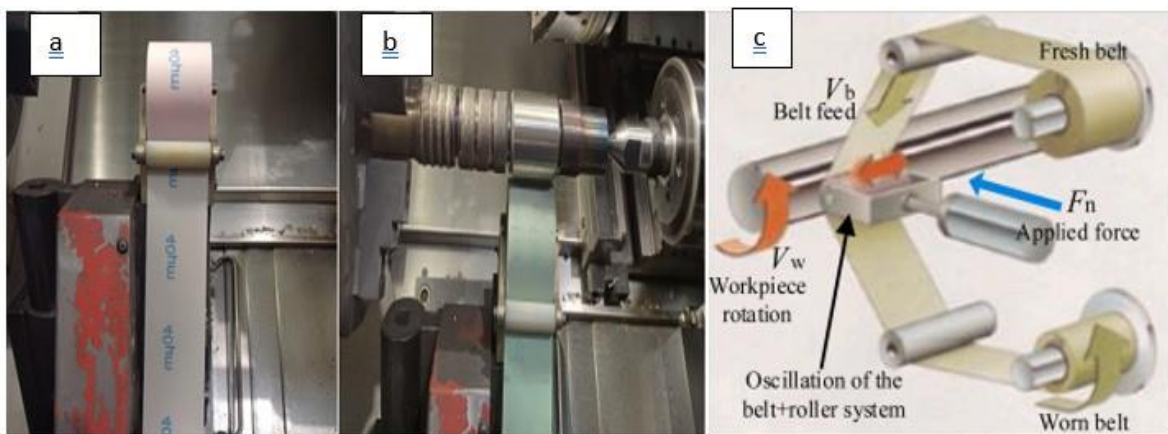


Figure 4.3: Belt and experimental setup (a) 40 μm , (b) 80 μm and (c) working principle [15]

4.3.4 | Surface Topography Measurement

In addition, the experimental setup includes a contact profilometer to measure and assess the surface quality of the completed item. Accurate surface roughness measurements are made possible by this precision measuring tool, which adds to a thorough and comprehensive study. Surface roughness measurements are performed before the belt finishing process (after turning operation) and after the belt finishing process for different process times. Three measurements are taken for every condition and the average of the measurements are used for the discussion and analysis.



Figure 4.4: Contact profilometer

4.4 | Result and Discussion

4.4.1 | Effect of the Belt-Finishing Duration on the Surface Roughness

Data collected from several groups formed during transverse project lab were compared. Data from the groups indicate comparable values; therefore, considering the similarity of the data from the different groups, the Ra parameter of roughness was plotted from all of the group data; additionally, for further analysis, data that appeared to be preferable was examined since the process parameters were same for each group.

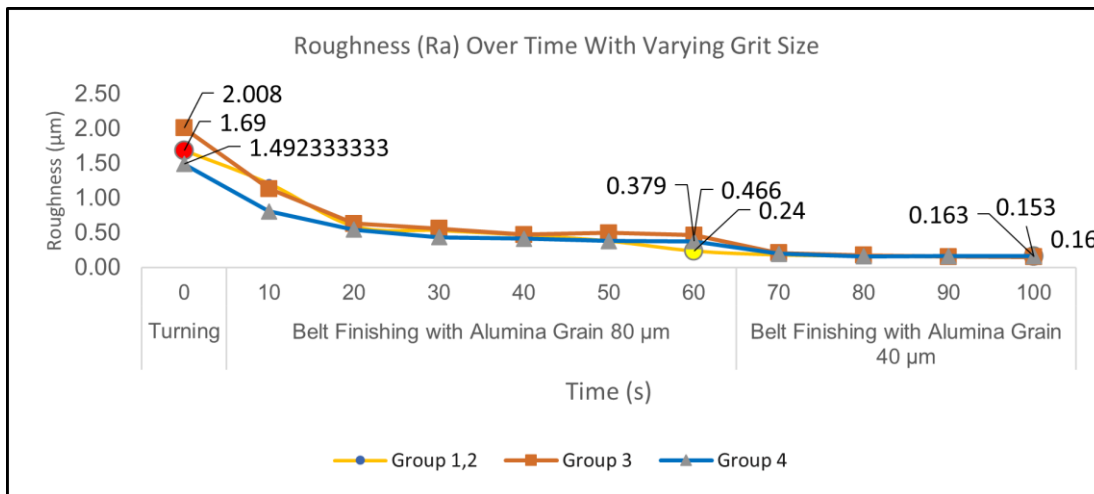


Figure 4.5: Variation of roughness with grain size and time

Belt-finishing operations require continuous reloading of active grains in the contact area due to the belt feed. New grains are brought in to the contact, while worn grains are removed, but the average number of active grains remains constant [20] [17]. According to the Figure.4.4.1 above the Ra value seems decreasing with increase in finishing time. The data from group 3 with the highest Ra value right after the turning process was used for further study. The various roughness and bearing parameters from group three study are presented below in the figure 4.6.

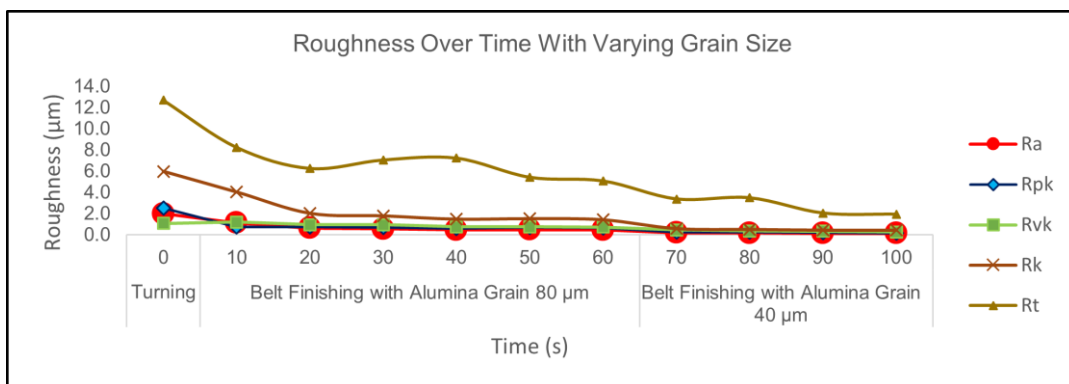


Figure 4.6: Variation of profile and bearing parameters with grain size and time

Considering the parameter 'Ra' is used as an international standard [20], it was extensively examined, considering the percentage Ra drop during the belt finishing process. The figure 4.4.3 below shows that belt finishing with 80 µm alumina abrasive grains reduced Ra from 2.008 µm to '0.466 µm, resulting in a 76% decrease 60 seconds. Additionally, utilizing 40 µm abrasive grain amounted to a 67% drop in Ra from 0.466 µm to 1.50 µm. The Rz parameter was also investigated. Belt finishing with 80 µm alumina abrasive grains reduced Rz from 10.50 µm to 4.15 µm, resulting in a 60% drop within 60 seconds. Additionally, using 40 µm abrasive grain resulted in a 63% reduction in Rz from 4.15 µm to 0.153 µm.

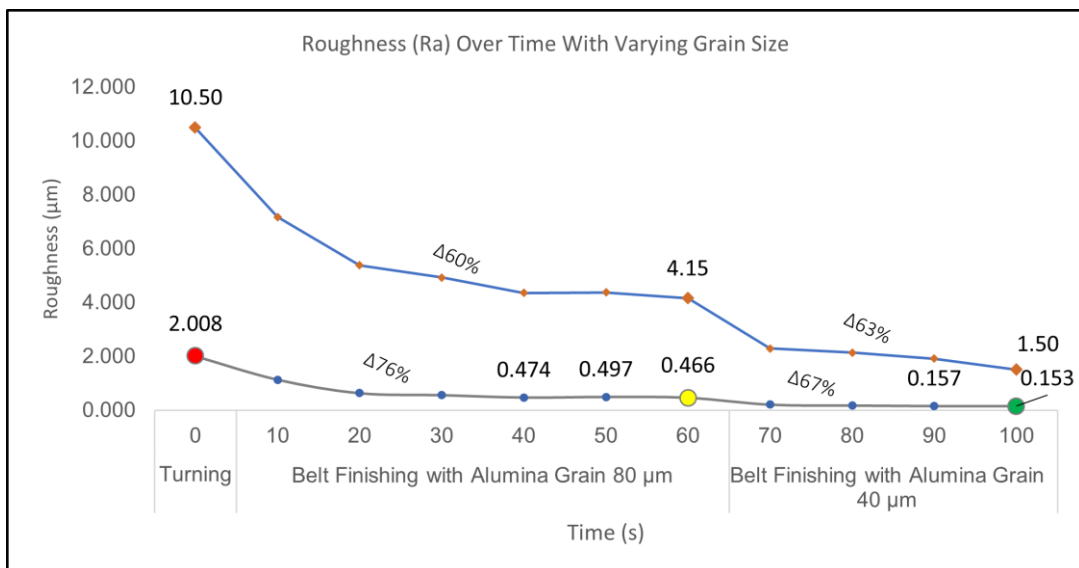


Figure 4.7: Percentage drop in roughness with grain size at end of 60s

Moreover, the percentage drop in Ra for both alumina grain sizes after each 10 seconds can be observed in the figure below. It can be seen that Ra drops significantly for the first 10-20 seconds then there is period of slow reduction followed by a period of stabilization shown in figure 4.8 below.

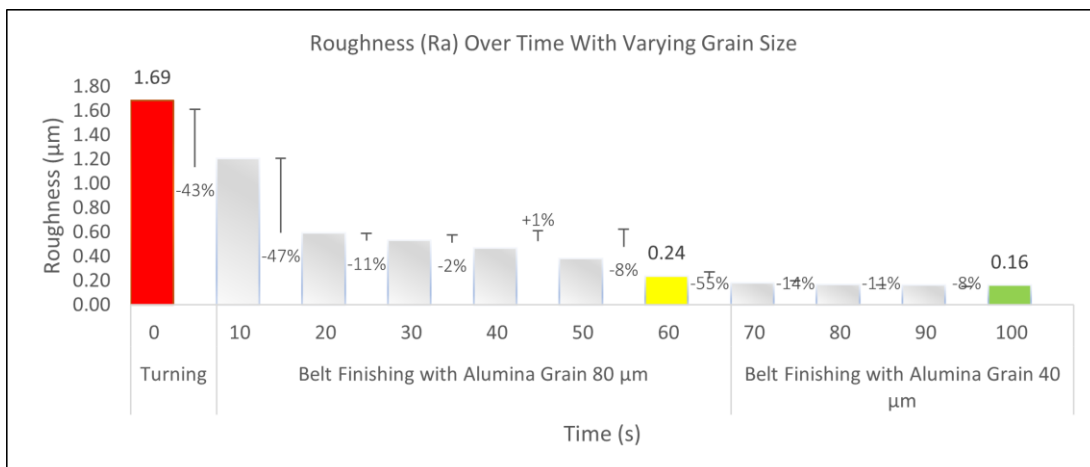


Figure 4.8: Percentage drop in roughness with grain size at end of each 10s

It was discovered that the smaller the abrasive grain size, the finer the Roughness Parameters, as shown in figure 4.9. The abrasive grain size can be chosen based on the application. Furthermore, some studies [21] demonstrated that employing an abrasive grain size of 9 μm enhanced the roughness parameter, indicating that an abrasive grain size of 20 μm or higher can be used for the belt finishing process depending upon desired roughness.

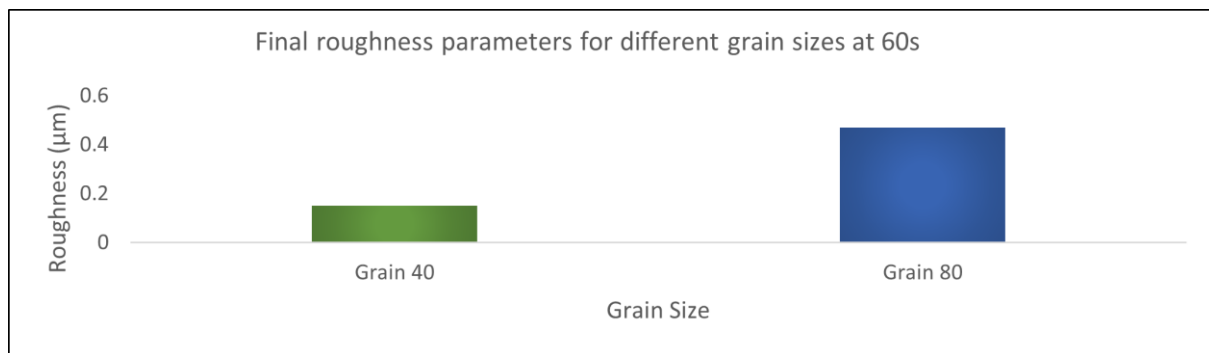


Figure 4.9: Roughness based on grain size after 60 of belt finish

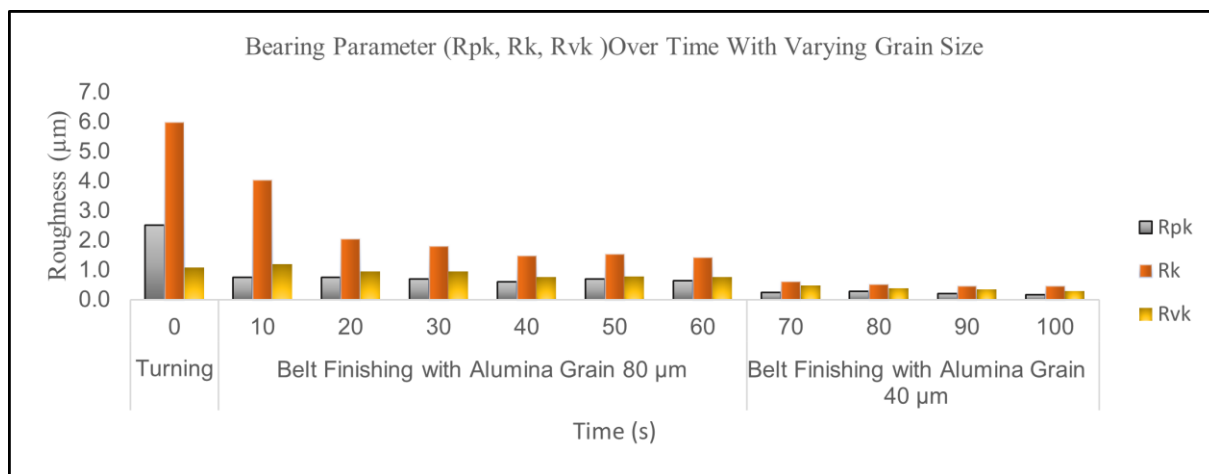


Figure 4.10: Influence of abrasive grain size on bearing parameters

Figure 4.10 shows that the three bars (Rpk, Rk, and Rvk) follow nearly identical trends; there is a relationship between the three parameters and the reduction in abrasive grit size. Belt finishing with 80 μm grain size reduces peak height Rpk by 76% compared to the initial Rp after 60 seconds, removing 24% of the peaks during the first 60 seconds of operation. Finishing with 40 μm grain size results in a 66% reduction of peaks after 40 seconds of operation removing 40% of the peaks during the first 40. This demonstrates that the running-in period can be as short as possible [8]. The final core roughness depth parameter Rk is approximately 76 and 64 percent lesser than the initial for fishing with belts of grain size 80 μm and 40 μm , respectively, indicating the material quantity available for wear [8]. The third parameter (reduced valley depth) Rvk is less than the initial state by about 27% and 40% for belts of grain size 80 μm and 40 μm , respectively. This leaves a small percentage of valleys those who will never be worn to retain the lubricant required for proper functioning.

4.5 | Conclusions

This study examined the effects of belt finishing processes on a turned SS 316L material, which was onto low-carbon steel through the process of laser cladding. Primarily, the influence of the belt-finishing duration on profile roughness and bearing parameters with different abrasive grain sizes (80 μm and 40 μm) was investigated. The following outcomes can be achieved:

- Belt finishing produces roughness profiles influenced by active grain geometries, distributions, and movements.
- Roughness profile characteristics and bearing parameters decrease with a reduction in grain size and an increase in time duration for the belt finishing process.
- Roughness profile features and bearing parameters decrease significantly over the first 10-20 seconds, followed by a period of steady reduction and stabilization. Thus, the belt-finishing surface approaches



the configuration that defines a plateau surface. This type of surface is essential due to its superior surface features and bearing properties.

- The above factors provide clear proof that belt finishing can be implemented for superfinishing steel deposited by laser cladding.
- Further research might be conducted to investigate the microstructural modifications and residual stress properties generated by the belt finishing process.

5 | Ball Burnishing

Authors: Barkin Aydin, Abhijith Brijesh Mohan, Jonathan Coro, Clinton Ikechukwu, Ugbine Oghenefegor F.

5.1 | Introduction

Ball burnishing, a post-machining technique, assumes a pivotal role in enhancing the surface characteristics and mechanical properties of machined metallic components. Employing a ball typically crafted from materials such as aluminium carbide, cemented carbide, or silicon nitride, under emulsion pressure, spanning a range of 80 to 200 bar. The ball's methodical rolling action across the surface, coupled with the application of a normal force exerts a pressure which impacts the surface integrity of a substrate. These enhancement signatures include induced plastic deformation, improved compressive residual stress and geometric parameters, notably surface roughness. The resultant synergy of these refinements collectively contributes to a substantial augmentation in the fatigue life of the treated metallic components [22]. Figure 5.1 shows a schematic representation of ball burnishing.

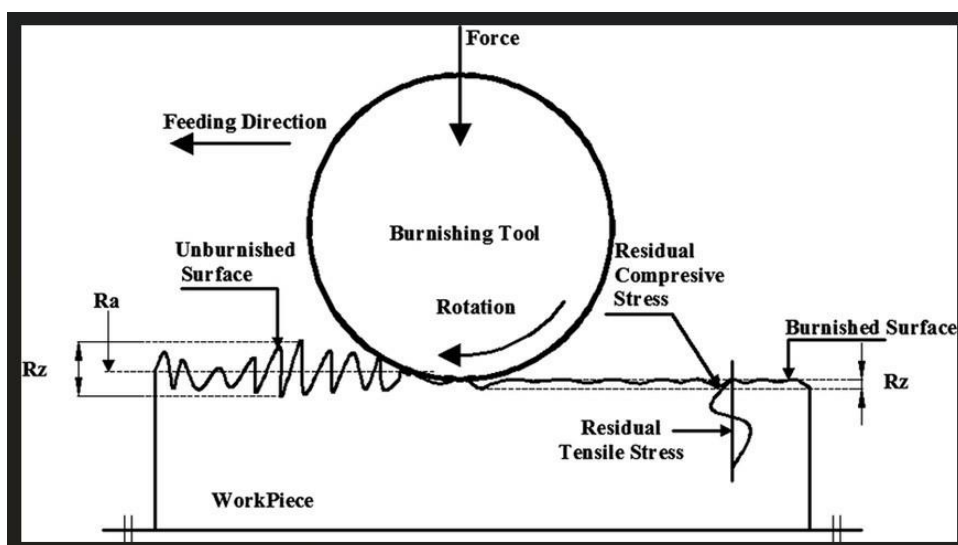


Figure 5.1: A schematic representation of ball burnishing [23].

5.2 | Objectives

The aim of this practical session is to control the roughness of the material SS 316L, deposited by laser cladding and cold spraying with the following objectives:

- Understanding how ball burnishing process works.
- To investigate the effect of ball burnishing on the surface roughness of laser-clad stainless steel 316L.
- To investigate the influence of feed rate of the ball burnishing process on the surface roughness of laser clad stainless steel.

5.3 | Materials and Method

Stainless steel 316L, previously deposited by laser cladding on a low-alloyed steel, 42CD4, served as the substrate for ball burnishing experiments conducted on a CNC lathe equipped with an Ecoroll setup and a 6mm diameter ball. Using parameters detailed in Table 5.1 (rolling speed: 120 m/min, normal force: 250 N, cutting fluid: emulsion). The maximum feed rate (0.2 mm/rev) were found on the catalogue of tool manufacturer [24]. Subsequently, semi-finishing turning operations, with a constant feed rate of 0.2 mm/rev, were performed on the bulk (0.2 mm depth of cut), 5-layer (1 mm depth of cut), and 1-layer (0.5 mm depth of cut) laser-clad configurations.

Table 5.1: Process Parameters for Ball Burnishing Operation.

Parameter	Unit	Value
Speed	mm/min	120
Load	N	250
Ball Diameter	mm	6
Pressure	bar	100

Table 5.2: Process Parameters for Turning Operation.

Parameter	Unit	Value
Cutting Speed V _c	mm/min	120
Feed (f)	mm/rev	0.2
Depth of cut (ap) for Bulk	mm	0.2
Depth of cut (ap) for 5 layer	mm	1
Depth of cut (ap) for 1 layer	mm	0.5



Figure 5.2: Ecoroll Tool Information.

5.4 | Results and Discussion

5.4.1 | Analysis of Laser Cladded 1-Layered Specimen

Table 5.3: Experimental and theoretical Ra values for ball burnishing.

Test	Feed (mm/rev)	a _p (mm)	V _c (mm/min)	R _a (μm)	R _a _{theo} μm	Variation %
1	0.17	1	120	0.276	0.309	11
2	0.17	1	120	0.258	0.309	17
3	0.17	1	120	0.258	0.309	17
4	0.05	1	120	0.243	0.0267	809
5	0.05	1	120	0.245	0.0267	817
6	0.05	1	120	0.198	0.0267	641
7	0.2	1	120	0.310	0.428	28
8	0.2	1	120	0.330	0.428	23
9	0.2	1	120	0.304	0.428	29
10	0.1	1	120	0.080	0.107	25
11	0.1	1	120	0.074	0.107	31
12	0.1	1	120	0.066	0.107	38

As we can see from the Table 5.3; the theoretical Ra values are matching with the experimental Ra values. But, on test numbers 4, 5, and 6 which have feed rates of 0.05 mm/rev, there is a large difference between theoretical and experimental values. Our experimental values were significantly higher than the theoretical values. This was unexpected. We think that the reason for this big difference is laser cladding creates a non-homogeneous surface. In addition, the reason for the low roughness values in the tests performed with 0.1 mm/rev feed rate is that the measurement length of the stylus profilometer for those readings were smaller compared to other measurements (3.5 mm instead of 4.8 mm).

Table 5.4: Experimental and theoretical Ra values for turning.

Test	Feed (mm/rev)	a _p (mm)	V _c (mm/min)	R _a (μm)	R _a _{theo} (μm)	Variation %
1	0.2	1	120	1.945	1.604	21
2	0.2	1	120	1.783	1.604	11
3	0.2	1	120	1.846	1.604	15
4	0.2	1	120	1.729	1.604	8
5	0.2	1	120	1.677	1.604	5
6	0.2	1	120	1.734	1.604	8

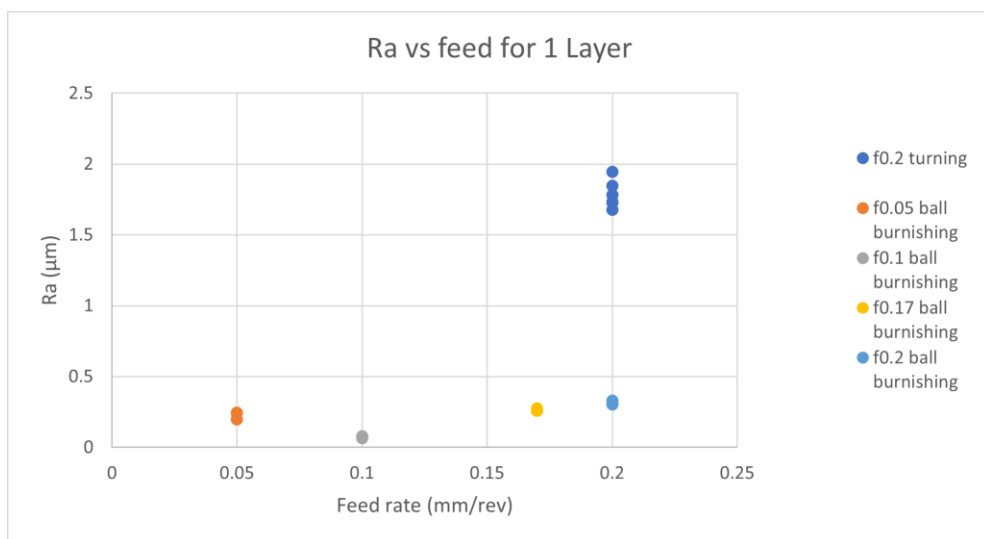


Figure 5.3: Ra vs feed rate graph for laser cladded 1-layer specimen.

Figure 5.3 shows the variation of Ra over feed rate for the single layer cladding. From the plot, it is observed that ball burnishing reduces the average roughness parameter (Ra) compared to the initial turned sample. It is also seen that as the feed rate is decreased during the ball burnishing process, the Ra decreases. However, when decreasing from $f=0.1$ mm/rev to $f=0.05$ mm/rev, it is observed that the Ra increases. This is in contradiction with the theoretical average roughness that was calculated, which was expected to further decrease.

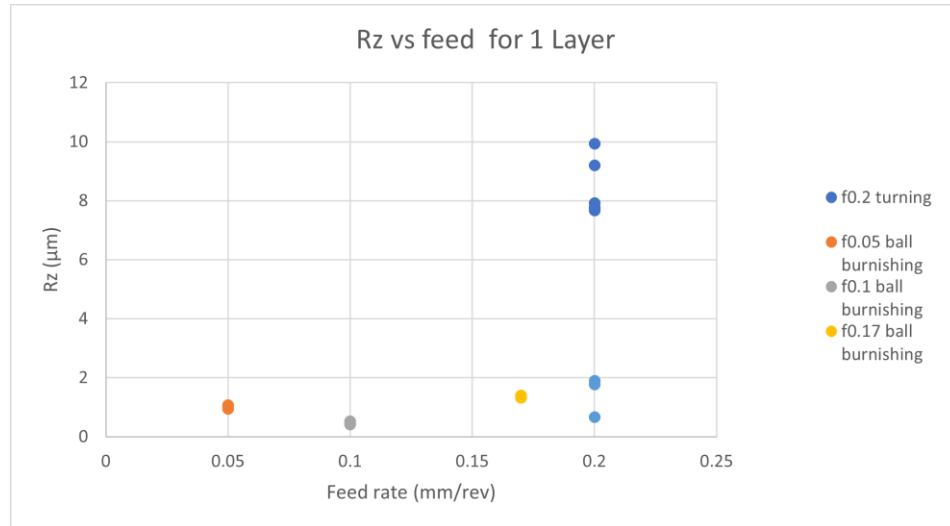


Figure 5.4: Rz vs feed rate graph for laser cladded 1-layer specimen.

Figure 5.4 shows the variation of Rz over the feed rate. This plot also shows a similar trend to the variation of Ra over feed. So, the effect of ball burnishing is to decrease the value of Rz compared to the turned sample. Similarly, the Rz also increases when the feed rate was varied from 0.1 mm/rev to 0.05 mm/rev.

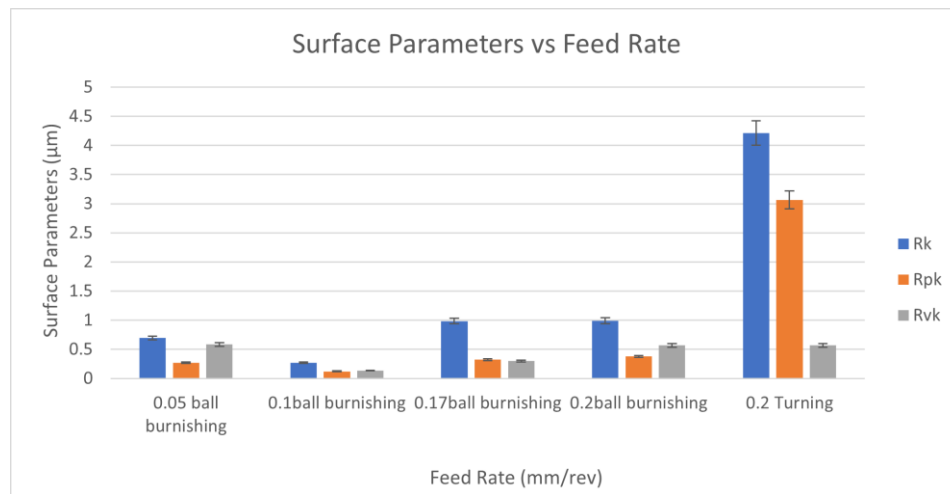


Figure 5.5: Surface parameters vs feed rate graph for laser cladded 1-layer specimen.

The same trend is followed for the Abbott-Firestone parameters (Rk, Rpk, and Rvk). The parameters decrease due to the ball burnishing compared to the turned sample. And as earlier observed for the Ra and Rz values, these parameters also initially decrease as the feed rate is reduced, but increase when the feed rate is further reduced from $f=0.1$ mm/rev to $f=0.05$ mm/rev. We propose the reason for the decrease in roughness parameters observed when the feed rate is further lowered is that the lower feed of 0.05 mm/rev does not affect the signature of the clad surface and therefore, the roughness does not decrease, but rather, increases.

5.4.2 | Analysis of Laser Cladded 5-Layered Specimen

Table 5.5: Experimental and theoretical Ra values for turning.

Test	Feed (mm/rev)	a_p (mm)	V_c (mm/min)	$R_a(\mu m)$	$R_{a\text{theo}}(\mu m)$	Variation %
1	0.2	1	120	1.484	1.6038	7
2	0.2	1	120	1.473	1.6038	8
3	0.2	1	120	1.48	1.6038	8
4	0.2	1	120	1.815	1.6038	13
5	0.2	1	120	1.879	1.6038	17
6	0.2	1	120	1.875	1.6038	17
7	0.2	1	120	1.865	1.6038	16
8	0.2	1	120	1.837	1.6038	15
9	0.2	1	120	1.754	1.6038	9
10	0.2	1	120	1.716	1.6038	7
11	0.2	1	120	1.745	1.6038	9

Table 5.6: Experimental and theoretical Ra values for ball burnishing.

Test	Feed (mm/rev)	a_p (mm)	V_c (mm/min)	$R_a(\mu m)$	$R_{a\text{theo}}(\mu m)$	Variation %
1	0.05	1	120	0.303	0.0267	1034
2	0.05	1	120	0.283	0.0267	959
3	0.1	1	120	0.188	0.1069	76
4	0.1	1	120	0.162	0.1069	52
5	0.15	1	120	0.263	0.2406	9
6	0.15	1	120	0.287	0.2406	19
7	0.2	1	120	0.299	0.4277	30
8	0.2	1	120	0.324	0.4277	24
9	0.2	1	120	0.323	0.4277	24
10	0.2	1	120	0.3	0.4277	30
11	0.2	1	120	0.327	0.4277	24
12	0.1	1	120	0.289	0.1069	170
13	0.1	1	120	0.277	0.1069	159
14	0.1	1	120	0.28	0.1069	162

Table 5.6 shows the Ra values for the ball burnished five-layer clad surface. Most of the tests shows a good match between the experiment and theoretical Ra values. However, for tests 1 and 2, there is a large variation between the experimental and theoretical roughness values, which was also observed for the single layer clad for the feed rate of 0.05 mm/rev.

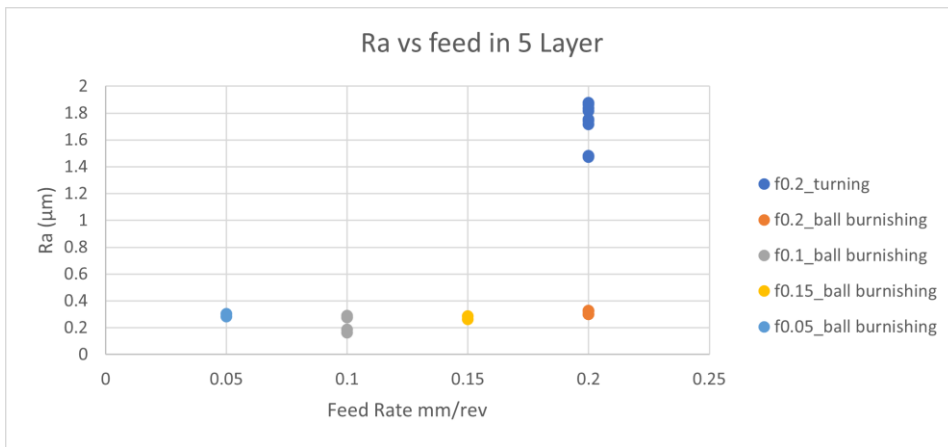


Figure 5.6: Ra vs feed rate graph for laser cladded 5-layer specimen.

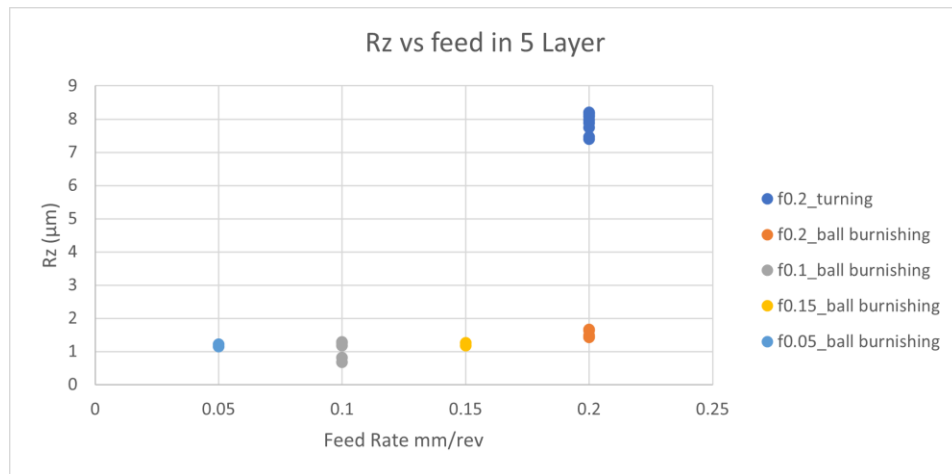


Figure 5.7: Rz vs feed rate graph for laser cladded 5-layer specimen.

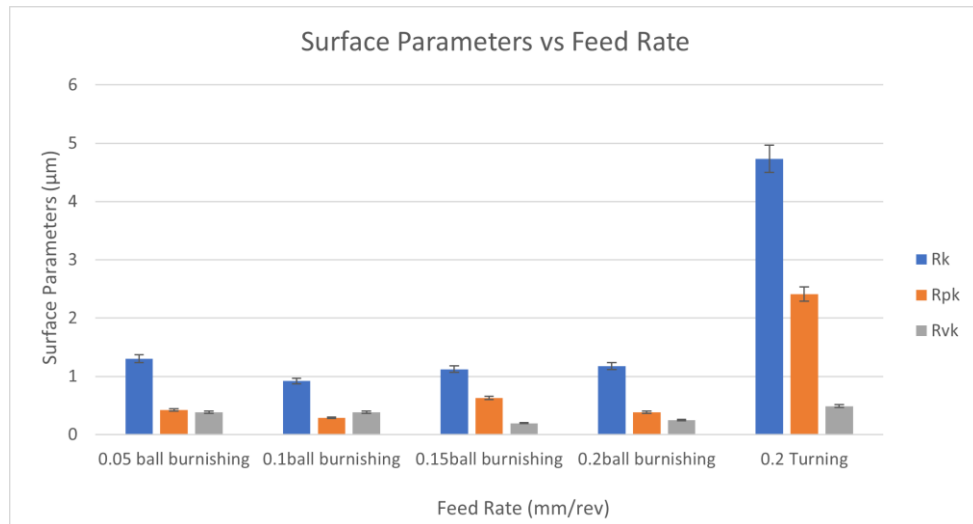


Figure 5.8: Surface parameters vs feed rate graph for laser cladded 5-layer specimen.

For the five-layer clad surfaces as well, the roughness parameters show the same trend as was observed for the single layer clad surfaces. By ball burnishing, the roughness parameters are decreased compared to the initial values for the turned samples. Similarly, the parameters all decrease while decreasing the feed rate of the ball burnishing initially. However, the values increase (instead of the expected decrease) when the feed rate is lowered from $f=0.1 \text{ mm/rev}$ to $f=0.05 \text{ mm/rev}$.

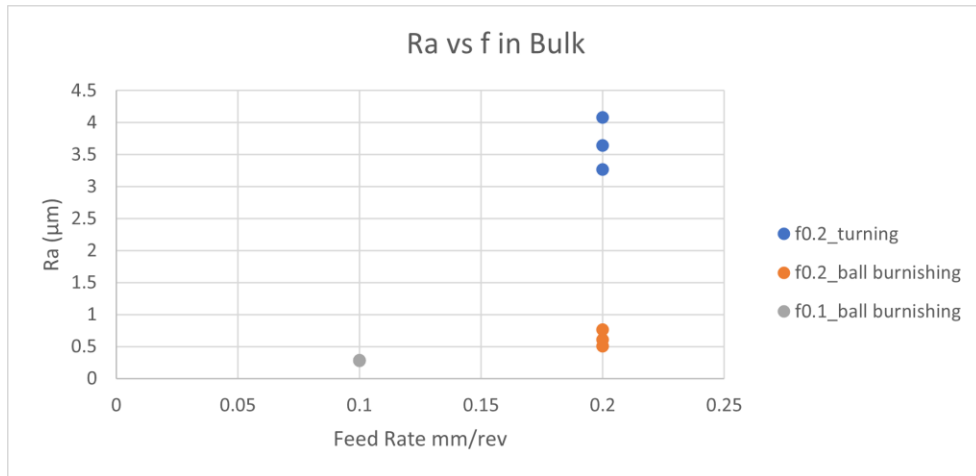
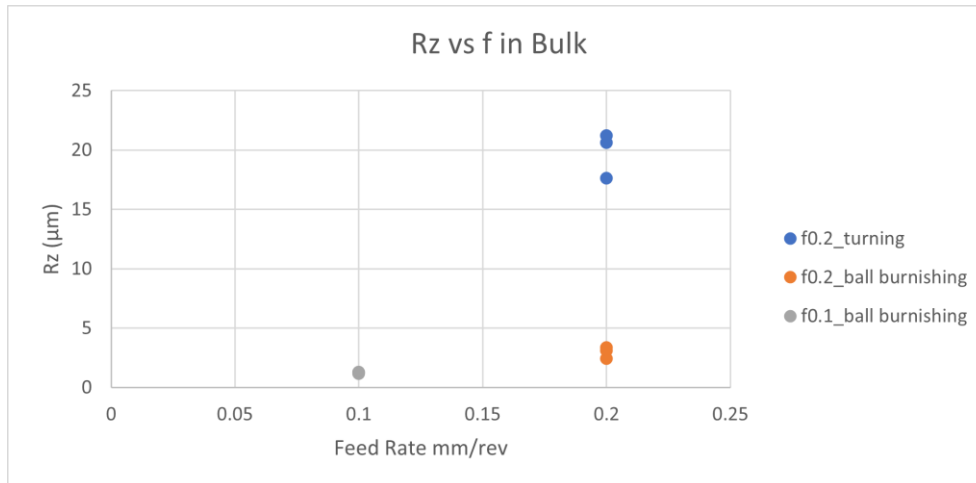
5.4.3 | Analysis of Substrate (Bulk) surface

Table 5.7: Experimental and theoretical Ra values for turning.

Test	Feed (mm/rev)	a_p (mm)	V_c (mm/min)	$R_a(\mu\text{m})$	$R_{a\text{theo}}(\mu\text{m})$	Variation %
1	0.2	1	120	3.646	1.604	127
2	0.2	1	120	3.267	1.604	104
3	0.2	1	120	4.084	1.604	155

Table 5.8: Experimental and theoretical Ra values for ball burnishing.

Test	Feed (mm/rev)	a_p (mm)	V_c (mm/min)	R_a (μ m)	$R_{a\text{theo}}$ (μ m)	Variation %
1	0.2	1	120	0.762	0.4277	78
2	0.2	1	120	0.51	0.4277	19
3	0.2	1	120	0.607	0.4277	42
4	0.1	1	120	0.289	0.1069	170
5	0.1	1	120	0.277	0.1069	159
6	0.1	1	120	0.28	0.1069	162


Figure 5.9: Ra vs feed rate graph for bulk specimen.

Figure 5.10: Rz vs feed rate graph for bulk specimen.

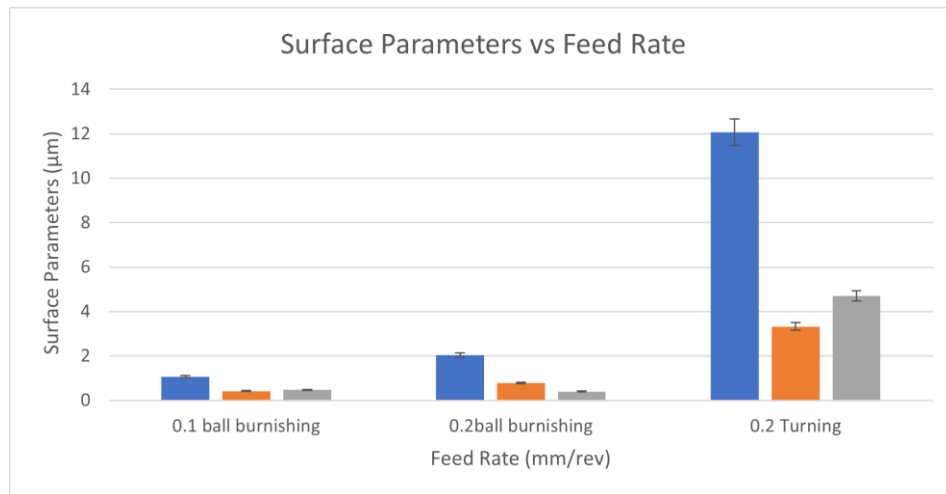


Figure 5.11: Surface parameters vs feed rate graph for bulk specimen.

Tests were also carried out on the bulk sample, which does not contain any cladding. While comparing the effect of ball burnishing to turning, it is observed that the roughness parameters all decrease for the burnished surface compared to the turned surface.

The effect of changing the feed rates was also studies for two feed rates, $f = 0.2 \text{ mm/rev}$ and 0.1 mm/rev . By decreasing the feed rates, the roughness parameters were all observed to decrease. Since these tests were not done for the feed rate of 0.05 mm/rev , it is not known whether the previously observed anomaly of the increased roughness for $f = 0.5 \text{ mm/rev}$ would have been observed for this sample as well.

5.4.4 | Analysis of Cold-Sprayed Surface

Two types of materials (copper and stainless steel) were coated on to the aluminium substrate. After several turning trials smooth surface could not be obtained (see in Figure 5.12). This is because during cold spray, the coating becomes very hard due to the high deformation. Even though turning was tried many times with different parameters, they all failed. A smooth surface could not be obtained and the cutting tool broke. Therefore it could not be machined unless prior heat treatment was done. Due to the lack of time the heat treatment process could not done.

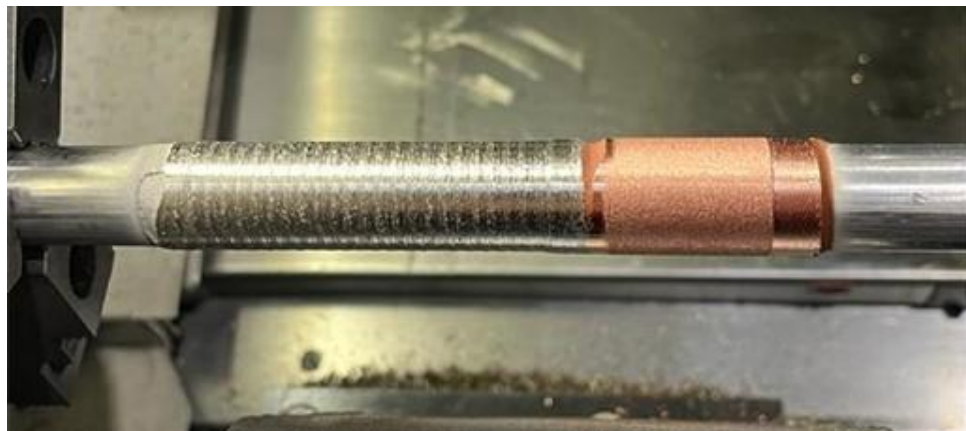


Figure 5.12: Cold-sprayed specimen after several turning process.



5.5 | Conclusion

The experiments were carried out to study the ball burnishing process, to understand the effect of ball burnishing a surface compared to turning, and the effect of varying the feed rates for the ball burnishing. When ball burnishing is carried out, all the roughness parameters studied (R_a , R_z , R_k , R_{pk} , R_{vk}) decreased compared to the sample on which only turning was done. This is expected from the process, as it deforms and smoothes the surface.

Theoretically, the roughness parameters are expected to decrease when the feed rate for ball burnishing is lowered. This was observed for some feed rates. However, on the experiments done on the laser clad samples, there is an increase in the roughness parameters when the feed was decreased to 0.05 mm/rev. This is attributed to the feed not affecting the signature of the clad surface due to the inherent non-homogeneous nature of the laser cladding process.

However, due to the lack of tests done at $f=0.05$ mm/rev for the substrate alone (as tests were only done down to feed rates of 0.1 mm/rev), we cannot conclusively decide whether the increase in the roughness values is observed only for the cladding or whether the same trend would have been observed for the substrate as well.

To conclude, ball burnishing is an excellent process to utilize to obtain good surface finish. However, more tests could be done at lower feed rates in the future to conclude properly about the deviation from the theoretical roughness that is observed at lower feeds



6 | Surface Topography Characterization

Authors: Shah Saud, Muteeb Ur Rehman Rao, Sachintha Banuka, Anika Shama, Saikrishna Suresh Kumar

6.1 | Introduction

The surface of a solid delimits its volume and defines the region where interactions with its environment occur. The most straightforward explanation about the surface is the boundary between air and material. Surface topography characterization involves the systematic study and analysis of the physical features and variations present on the surface of a material or object. The motivation is to comprehensively understand, quantify, and describe the surface's form, roughness, and waviness. This process is crucial for various scientific, engineering, and industrial applications, as surface topography directly impacts the functionality and performance of materials. The characterization provides valuable information for optimizing material properties, ensuring product quality, and enhancing performance in specific applications.

Surface roughness is a second-order effect. Surface profiles are generated due to manufacturing technology used to produce surfaces. When the surface is generated, evaluating whether it has the required parameter to function when the first-order problem is solved is necessary. The four scales to characterize the functionality and integrity of the surface are[25]:

1. Shape
2. Waviness
3. roughness
4. Micro-roughness

Waviness of a surface refers to variations in the surface profile that occur on a larger scale than roughness but smaller than form. In waviness, the distance between two peaks is less than 1mm. Roughness is smaller than waviness but larger than micro roughness. The distance between the two peaks is less than 0.1mm. Micro roughness refers to the variation of the surface with a distance between peaks less than 0.01mm.

As discussed in Chapter 4 subsection 4.1.2, Average Roughness (R_a) is a crucial parameter among amplitude parameters. Total roughness (R_t) refers to the height difference within a particular length. (R_z) is a surface roughness parameter that measures the average maximum height of the peaks and valleys within a specified sampling length on a surface. (R_{pk}) and (R_{vk}) are parameters used in the context of surface roughness measurements (R_{pk}) specifically measures the height of the primary peaks on a surface, and (R_{vk}) measures the valley on the surface.

Several techniques are used for surface characterization, providing insights into the topography. Standard methods for surface characterization include Stylus Instrument Interferometer, Confocal Microscope, Focus Variation Microscope, Scanning Electron Microscope, and Atomic Force Microscope. A confocal microscope and a focus variation microscope were used during our practical session.

Confocal Microscope is an optical imaging tool for obtaining high-resolution, three-dimensional specimen images. "confocal" refers to using a spatial pinhole to eliminate out-of-focus light, improving image clarity and depth resolution. This technique benefits biological and material science applications where detailed imaging of thin sections or live specimens is essential. The main advantages of confocal microscopes are they are adapted to smooth surfaces, have high lateral ($< 10\text{nm}$) and vertical resolution ($< 10\text{nm}$), are fast (few s), and have some drawbacks such as issues for non-reflective samples and vibration sensitivity[26].

Focus Variation Microscopy is an advanced optical microscopy technique for high-resolution three-dimensional surface profiling of specimens. This method provides precise surface topography measurements by utilizing the variation in focus across the specimen. It is precious for applications where accurate surface characterization is essential. Focus variation microscopes have unique advantages, such as adapting to rough surfaces, form measurements, and fast (few s), and some drawbacks, such as smooth surfaces without contrast.

6.2 | Objectives

- Analyze the 3D topography characteristics by non-contact techniques.
- Analyze the effect of super finishing techniques on roughness parameters.
- To use the effect of the Gaussian filter on the topography analysis.
- Analysis of waviness of Ball burnished and Belt finished surfaces.

6.3 | Material and Methodology

After the super-finishing processes on the laser cladding sample, three samples were selected for topography made at specific parameters to analyze the process signature on the surface:

1. Belt finished cladded sample- with 40 microns grains (BF 40)
2. Ball burnished clad sample- with feed rates of 0.05mm/min (BB 0.05), 0.1 mm/min (BB 0.1), 0.15 mm/min (BB 0.15), 0.2 mm/min (BB 0.2), and 0.1 mm/min × 5 times (BB 0.1x5).
3. Ball Burnished substrate at a feed rate of 0.1mm/min (SB 0.1)

The surface of both samples was analyzed by confocal microscope and focus variation microscope, as both analyzed the sample with different light interaction techniques.

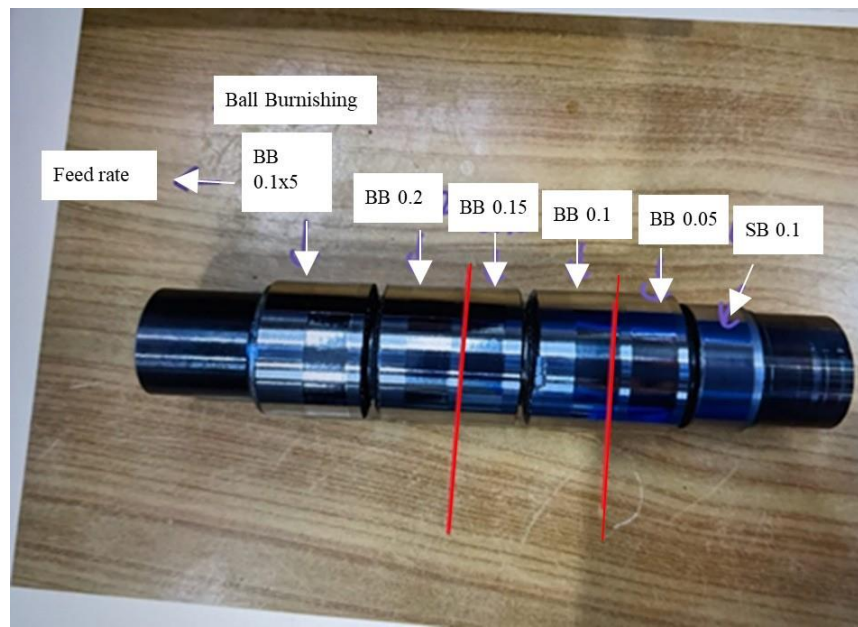


Figure 6.1: Cladded sample ball burnished at different feed

Confocal Microscope

Samples were placed under the confocal microscope using the specific sample holder, as shown in the figure. Under the bright field, the area position was selected for the analysis, which is of specific dimension 0.8mm by 0.6 mm. With a 20x lens under a confocal field, 50 to 60 microns were analyzed vertically with focus points between the range.

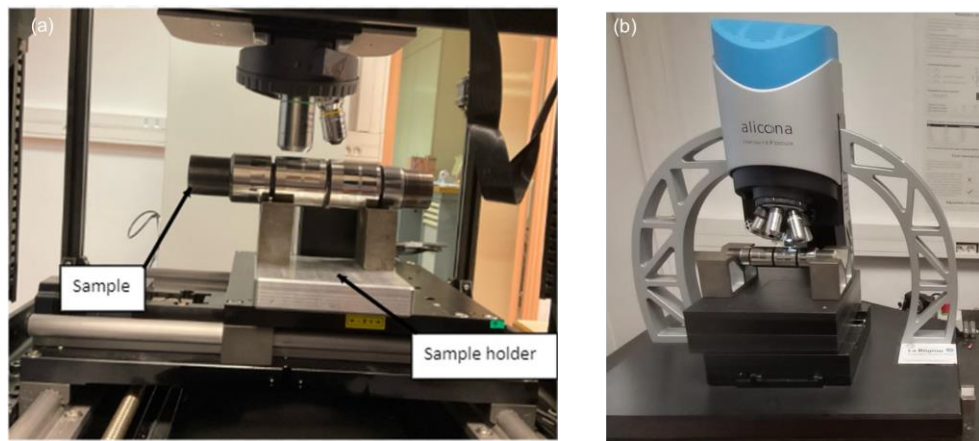


Figure 6.2: Cladded sample under (a) confocal microscope and (b) focus vision microscope

Focus vision microscope:

Samples were placed under alicona microscope one by one after proper cleaning with ethanol, as shown in Figure 6.2. It analyzes the surface along 1 to 5mm length, which can give good results statistically. After having the focus point, two defocus points were selected and marked randomly on each vertical side of the focus point to give the range of vertical analyzing movement.

Roughness parameters analysis:

After analyzing the samples with both microscopes, data was transferred to Mountains Map Expert software to analyze the roughness parameters. A template was created with an S-type filter to remove the shape form. It was designed to measure the roughness parameter values with a Gaussian filter of 0.6 and without any filter to observe the signature of the process. Data was stored in pdf form for observations and further analysis.

Overview of methodology for 3D topography is as follow:

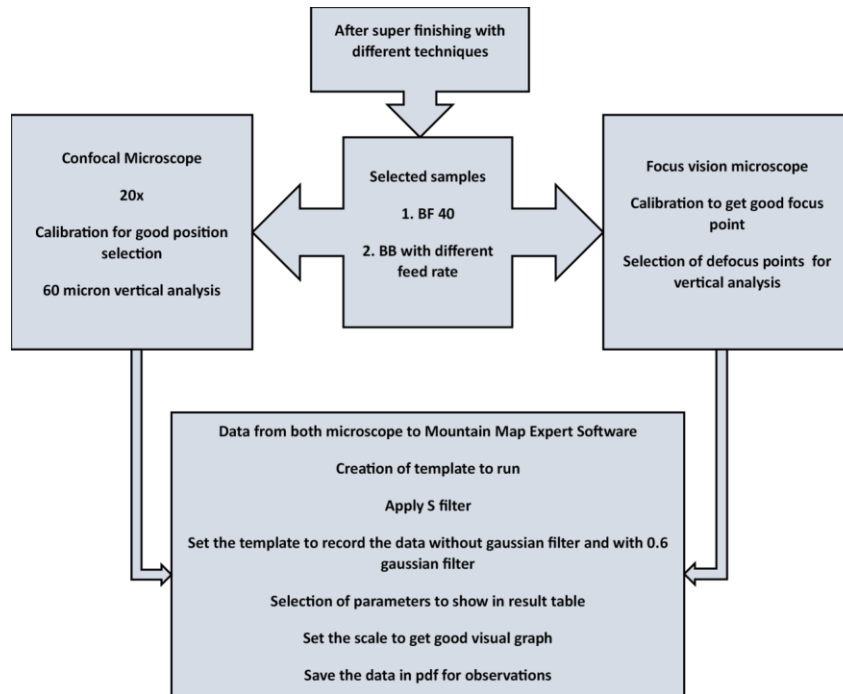


Figure 6.3: Overview of 3D topography methodology

6.4 | Results and Discussion

The 3D surface characterization techniques of confocal microscopy and focus variation microscopy help us visualize results that cannot be determined using stylus profilometry. Through these characterization techniques, we can filter data and obtain results about the form, waviness, and roughness of Ball burnished and Belt finished surfaces of the sample, which were laser cladding. Then, surface finishing was done using finish turning. It will help us to further differentiate between the functional properties generated on the surface using the two superfinishing techniques.

Although Belt finishing was performed using a belt with varying grain size and time, the surface characterized was super finished using a belt of grain size 40 μm (BF 40). For Ball Burnishing, the laser clad sample for super finished using different feed rates of 0.05 mm/min (BB 0.05), 0.10 mm/min (BB 0.1), 0.15 mm/min (BB 0.15), 0.2 mm/min (BB 0.2) and Ball burnished five times with a feed rate of 0.1 mm/min (BB 0.1x5). The substrate surface ball burnished at 0.1 mm/min feed rate (SB 0.1) and laser-clad surface Finish Turned with a feed rate of 0.2 mm/min (FT 0.2) were also characterized. The effect of varying the feed rate was observed using the 3D characterization techniques, and a comparison was also made with the results obtained using stylus profilometry.

6.4.1 | Confocal Micorscopy

The results obtained for Confocal microscopy acquire data from a sample size of 0.8 mm \times 0.6 mm on the surface. Each surface is characterized first without any filter and then with a filter to analyse the waviness and roughness separately. Table A.2 (A) shows the results obtained from the characterization without filtering.

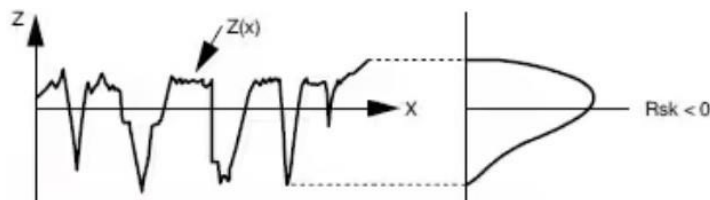


Figure 6.4: Surface Roughness Profile representation for $\text{Rsk} < 0$ [27]

It is important to note that for belt finishing, the value for Rsk is negative, which indicates the presence of deeper valleys and confirms that Belt finishes retain the signature of the original surface and just remove the peaks. This can also be confirmed by comparing the confocal microscopy profile.

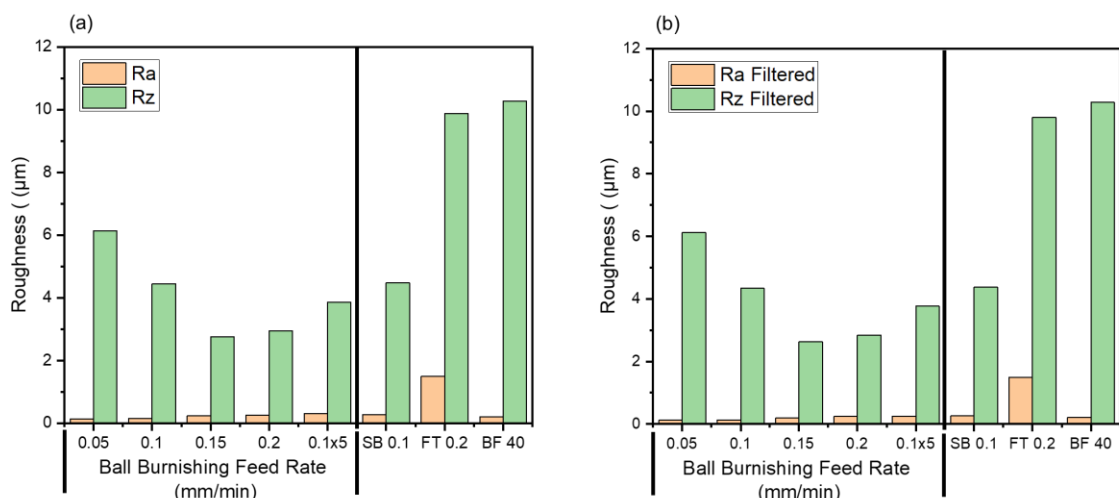


Figure 6.5: Comparison of Ra and Rz with ball burnishing (a) before and (b) after applying the filter

Filtering the results gives us a similar trend of an increase in Ra and a decrease in Rz with an increasing feed rate of ball burnishing, as shown in Figure 6.5.

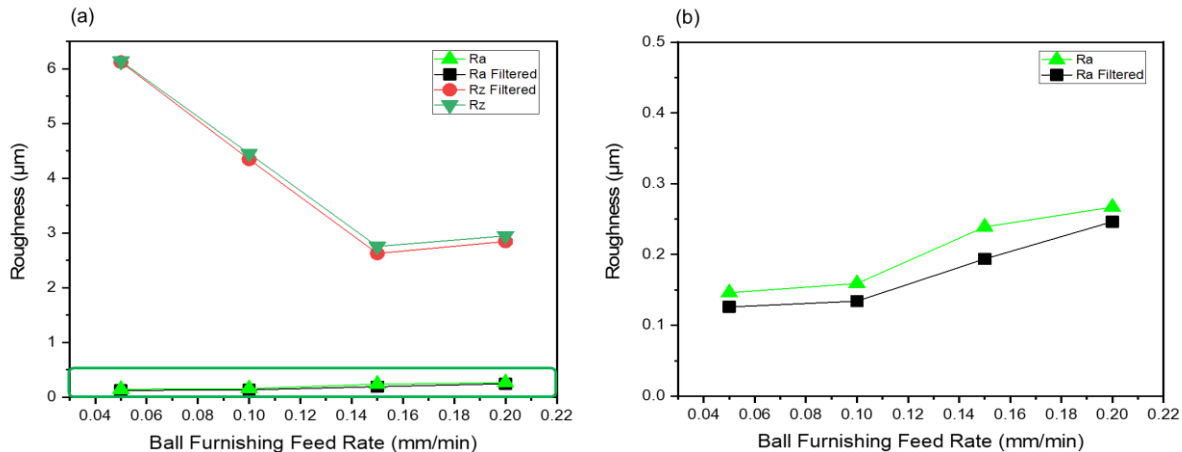


Figure 6.6: (a) Illustration of the relationship between Feed Rate and Surface Roughness (b) Zoomed-in graph for Ra and Ra filtered values.

In Figure 6.6, we can also look at the trend of increasing roughness with an increase in the feed rate. An increase in the feed rate leads to an increase in the deformation of a non-homogenous surface manufactured using laser cladding, and therefore, consequently, the surface roughness values increase.

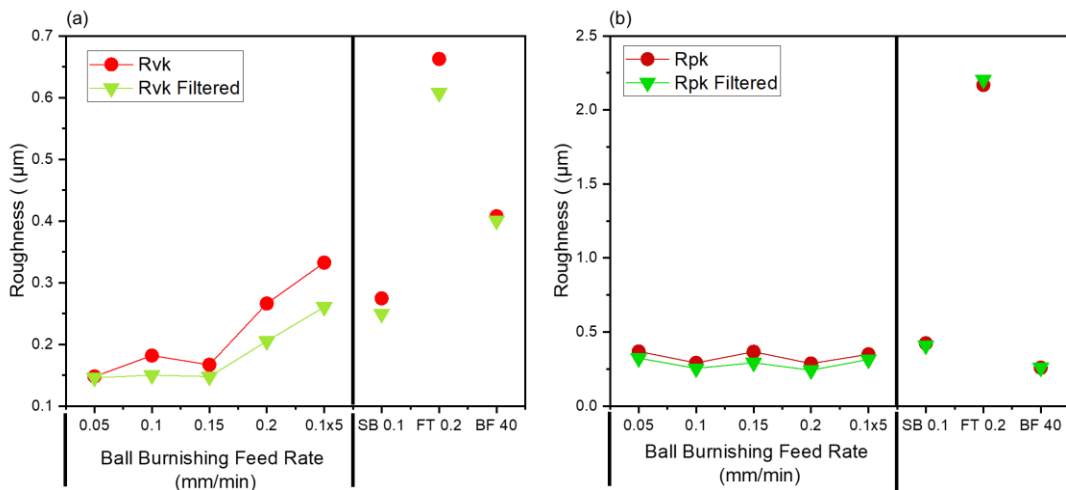


Figure 6.7: (a) Comparison of Rvk and Rvk filtered and (b) Comparison of Rpk and Rpk filtered with ball burnishing, Substrate, Finish turning, and Belt Finishing before and after applying the filter

Figure 6.7 shows the evolution of Rvk and Rpk's (unfiltered and filtered) roughness parameters over different feed rates of Ball Burnishing and for the substrate, finish turned, and Belt finished surfaces. We can observe that Rvk increases with the feed rate for ball burnishing. We can also observe that for BF 40, the Rvk is higher than Rpk, which indicates the removal of peaks but the retention of valleys on the surface profile.

Compared to the results obtained in Chapter 5.4.1 (Figure 5.3) with stylus profilometry, we can observe the values to be almost uniform. Hence, we can deduce that in stylus profilometry, the waviness induced onto the surface due to ball burnishing and laser cladding is filtered, giving us uniform roughness values with increasing feed rates. This is also validated by the topography profiles shown in Figure 6.8 and 6.11.

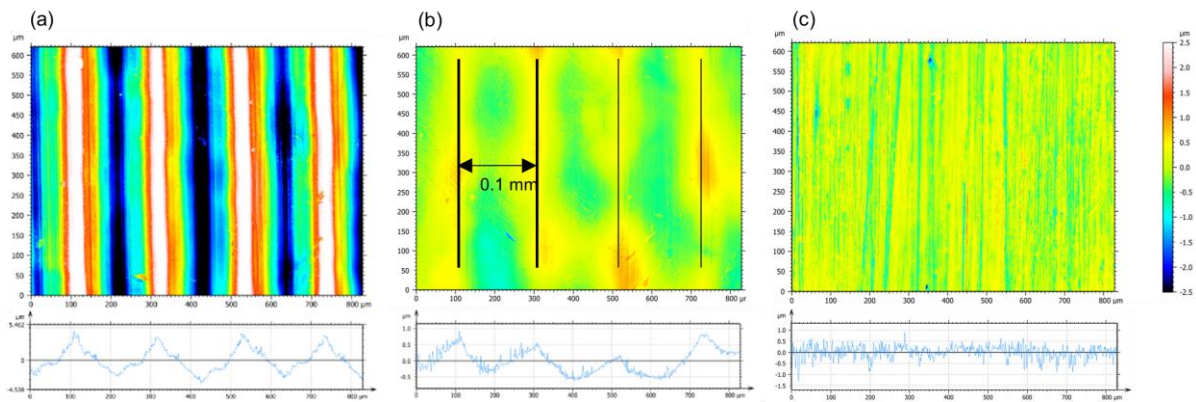


Figure 6.8: The topography image using confocal microscopy after (a) Finish Turning- FT 0.2 (b) Ball burnishing - BB 0.2 (c) and Belt finishing - BF 40

Looking at the topography image using confocal microscopy (Figure 6.8), we can closely observe the deformation tracks from the ball burnishing and the waviness profile of the surface. The variation indicates the Ball's diameter and the Ball's successive track. For the 3D plot of roughness for the BF 40 sample, we can observe that the waviness is not observed. This is attributed to the signature of the belt finishing process, which doesn't deform the surface but modifies the existing roughness of the surface by removing the peaks.

6.4.2 | Focus Variation

The results from focus variation microscopy measure the roughness profile over the area of 5 mm x 1 mm and, therefore, help us validate the results and analysis drawn from the confocal microscopy, where the surface area measured is relatively small.

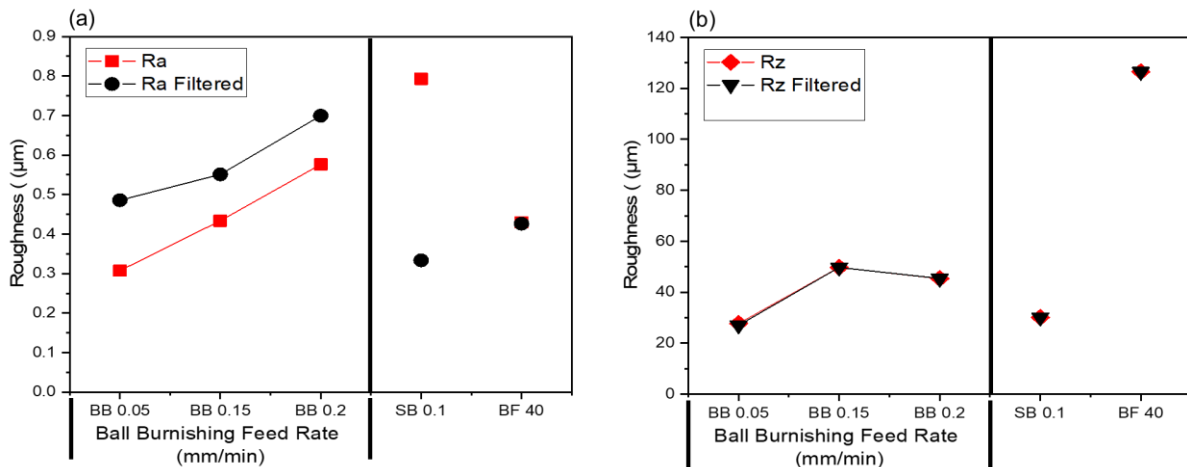


Figure 6.9: (a) Observation of Ra and (b) Rz with ball burnishing and before and after applying the filter

In Figure 6.9, for the Focus variation microscope, the mean roughness Ra and Rz values are higher than the ones obtained through Confocal Microscopy due to a larger sample area accounting for a more realistic surface picture. We can also see that filtering the data removes the waviness from the ball burnishing and the laser cladding tacks.

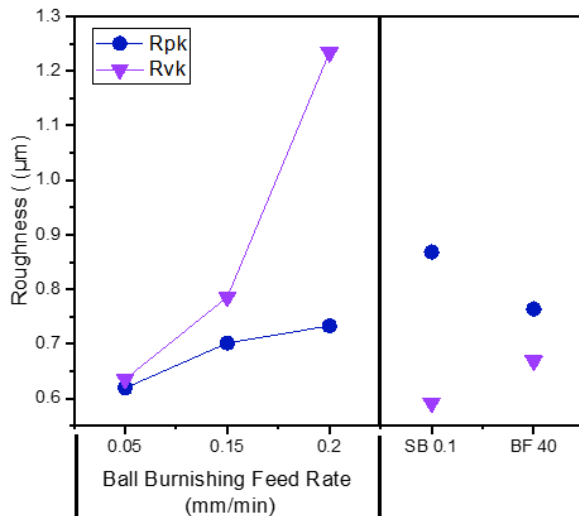


Figure 6.10: Observation of Rvk and Rpk with ball burnishing

We can also clearly distinguish between Rpk and Rvk values for ball burnishing and belt fishing (Figure 6.10). Rvk values for Ball Burnishing are higher, indicating that plastic deformation impacts creating valleys and functionalizing the surface. This effect is enhanced by increasing the feed rate. For Belt Finishing, we can observe that compared to the results from SB 0.1, the Rpk value has decreased, and the value for Rvk has increased. This again indicated the removal of peaks and increase of valleys but retention of the roughness signature from the original substrate[25].

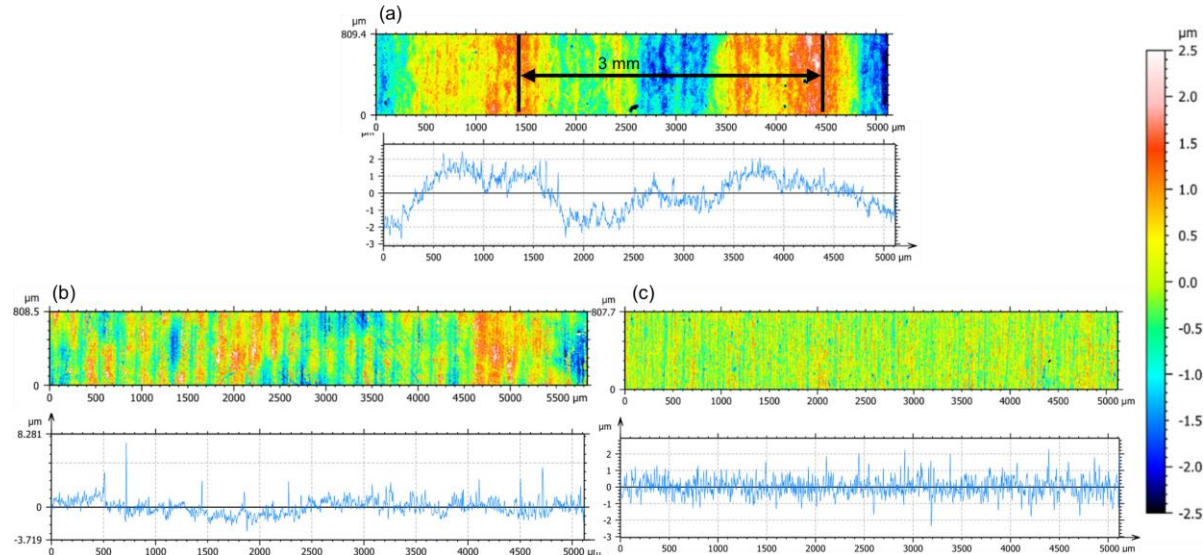


Figure 6.11: Roughness and topography profile of (a) Ball Burnishing Substrate - SB 0.1 (b) Ball Burnished of Cladded Sample - BB 0.2 (c) Belt Finished Sample BF 40

The larger the scanning area, the more insignificant the waviness due to the Ball burnishing path in the roughness profile, as seen in Figure 6.11. Although the waviness in the 2D plot cannot be observed on the 3D plot, we can still observe the ball burnishing tracks on the surface characterized. Moreover, Figure 6.11(a) shows the waviness of the surface, which can be attributed to the laser cladding single track width, which was approximately three mm[28].



6.5 | Conclusion

3D measurements were made for mapping Surface Topography using Confocal Microscopy and Focus Variation Microscopy on Ball Burnished, and Belt finished samples of laser clad with Stainless steel 316L on C45 Steel within the experimental limitations based on the details and its principle as discussed. The signature observed is that as the feed rate increases, the roughness parameter Ra increases. Meanwhile, Rz tends to decrease and increase for the Ball Burnishing operation with 3D measurements. There is a variation among the values obtained from the 2D profilometer for Ra and Rz for both operations, which has been well documented separately in the previous two chapters, which occurs due to the difference in the Gaussian filter being set at 0.8 by default by the device. There is a big difference in values obtained for the two processes on ball burnishing samples with and without a filter. The filter value is 0.6 among the two available options, 0.6 & 0.8, as the field area to analyze, is short(0.8mm X 0.6mm) for Confocal Microscopy with magnification set at 20X compared to Focus Variation Microscopy(5mm X 1mm). Similar is the trend for Belt finishing 40-micrometer grit size with the Gaussian filter, which contributes to the difference but has been used to compensate for the defects and abnormalities and remove the form and waviness from the scanned surface observed with the line graph. The Belt finished surface is observed to be slightly rougher than the ball-burnished surface. When the skewness parameter Ssk is negative(-ve), the valley is more dominant than the peak over the area. Shiny Surfaces can still have Waviness and roughness. Some values have not been recorded due to time constraints.



7 | Conclusion

To conclude generally, the key takeaways from the Transverse Project in Engineering include:

■ Transverse Practical Lab Work

- While learning how to connect different components of practical work. We started our lab work with the basics of powder characterization used for additive manufacturing techniques like laser cladding. Understanding which powder morphology is suitable for the process and the powder synthesis process required to achieve the optimal morphology. i.e., Plasma Spheroidization.
- After characterization, the powder was utilized in laser cladding. We learned how to optimize and control the parameters for laser cladding for optimal coating.
- Once we coated the substrate using laser cladded, we machined the surface using finished turning and super finished it using belt finishing and ball burnishing.
- To conclude, we characterized the surface integrity of our coating 2D (Stylus Profilometry) and 3D (Confocal Microscopy and Focus Variation Microscopy) characterization techniques used by measuring various roughness parameters.
- Qualitative difference between the results obtained from different characterization techniques was also analyzed.

■ Overall Results and Analysis

- **Powder Characterization:** Powder particles that have been developed by plasma spheroidization (S) present overall better properties such as a higher flowability, increased apparent and tap density, a more rounded shape, and a slightly smaller particle size distribution, in comparison to those that have been obtained by gas atomization (NS).
- **Laser Cladding:** The deposition properties can be enhanced by tuning the powder feed rate overlap process parameters.
- **Belt Finishing:** The surface roughness parameters decline with increasing belt finishing time, reaching a plateau at a specific duration. This plateau duration is a characteristic signature for each belt grain size, differentiating its polishing ability.
- **Ball Burnishing:** Ball burnishing decreases roughness compared to turning. The feed rate during ball burnishing is the key parameter responsible for the roughness obtained finally. Also, it is examined that surface homogeneity has an effect on resultant surface roughness.
- **Surface Topography Characterization:** 3D surface characterization techniques helped to determine the different waviness and form of the surfaces of ball burnished, belt finished and finished turned samples. They also allow us to collect unfiltered roughness values for different parameters, which is not observable in stylus profilometry. As a result, an increase in surface roughness was observed with an increase in feed rate, which was otherwise relatively uniform when recorded through the stylus profilometer.

■ Team Work and Collaboration

- Learning how to divide work and tasks related to report writing and compilation among 25 people.
- Compiling and sorting relevant data collected during practical work spanning over the course of 6 lab sessions.
- Learning patience and tolerance while understanding differences in work ethics.



8 | References

- [1] T. M. Abu-Lebdeh, G. P.-d. Leo'n, S. A. Hamoush, R. D. Seals, and V. E. Lamberti, "Gas atomization of molten metal: Part ii. applications," *American Journal of Engineering and Applied Sciences*, vol. 9, no. 2, Apr 2016.
- [2] G. Chen, S. Zhao, P. Tan, J. Wang, C. Xiang, and H. Tang, "A comparative study of ti-6al-4v powders for additive manufacturing by gas atomization, plasma rotating electrode process and plasma atomization," *Powder Technology*, vol. 333, pp. 38–46, 2018. [Online]. Available: <https://www.sciencedirect.com/science/article/pii/S0032591018302857>
- [3] N. Nkhasi, W. du Preez, and H. Bissett, "Plasma spheroidisation of irregular ti6al4v powder for powder bed fusion," *Metals*, vol. 11, no. 11, 2021. [Online]. Available: <https://www.mdpi.com/2075-4701/11/11/1763>
- [4] J. Li, Z. Hao, Y. Shu, and J. He, "Fabrication of spherical ti–6al–4v powder for additive manufacturing by radio frequency plasma spheroidization and deoxidation using calcium," *Journal of Materials Research and Technology*, vol. 9, no. 6, pp. 14 792–14 798, 2020. [Online]. Available: <https://www.sciencedirect.com/science/article/pii/S223878542031913X>
- [5] O. D. Neikov and N. A. Yefimov, "Powder characterization and testing," *Handbook of Non-Ferrous Metal Powders*, 2019. [Online]. Available: <https://api.semanticscholar.org/CorpusID:220126568>
- [6] E. W. Olson, "Particle shape factors and their use in image analysis – part 1 : Theory," 2013. [Online]. Available: <https://api.semanticscholar.org/CorpusID:2176233>
- [7] Z. Liu, "4.09 - laser applied coatings," in *Shreir's Corrosion*, B. Cottis, M. Graham, R. Lindsay, S. Lyon, T. Richardson, D. Scantlebury, and H. Stott, Eds. Oxford: Elsevier, 2010, pp. 2622–2635. [Online]. Available: <https://www.sciencedirect.com/science/article/pii/B9780444527875001414>
- [8] A. D. Découpe. (Accessed 2024-02-5) 42cd4 composition chimique et propriétés. [Online]. Available: https://www.acier-detail-decoupe.fr/module/seq_alliages/pdf?nomAlliage=42CD4
- [9] U. P. Metals. (Accessed 2024-02-5) 316 stainless steels specifications. [Online]. Available: <https://www.upmet.com/sites/default/files/datasheets/316-316l.pdf>
- [10] S. Naegeler. (2021) What is laser cladding? the important facts and new technology innovations. Accessed on February 5, 2024. [Online]. Available: <https://laserweldingsolutions.com/what-is-laser-cladding-the-important-facts-and-new-technology-innovations/>
- [11] N. Vale, C. Fernandes, R. Santos, T. Abreu Santos, and S. Urtiga Filho, "Effect of laser parameters on the characteristics of a laser clad aisi 431 stainless steel coating on carbon steel substrate," *JOM*, vol. 73, 08 2021.
- [12] B. Carcel, A. Serrano, J. Zambrano Carrullo, V. Amigó, and A. Cárcel, "Laser cladding of tial intermetallic alloy on ti6al4v -process optimization and properties," *Physics Procedia*, vol. 56, p. 284–293, 2014.
- [13] P. Xu, L. Zhu, P. Xue, G. Meng, S. Wang, Z. Yang, J. Ning, and Q. Lan, "Multi-track alternated overlapping model suitable for variable laser cladding process parameters," *Surface and Coatings Technology*, vol. 425, p. 127706, 2021. [Online]. Available: <https://www.sciencedirect.com/science/article/pii/S025789722100880X>
- [14] G. Lian, K. Yue, Z. Liu, H. Lu, and Y. Wang, "Influences of the cladding method and overlapping rate on the multi-channel overlapping of composite coatings," *Optik*, vol. 283, p. 170896, 2023. [Online]. Available: <https://www.sciencedirect.com/science/article/pii/S0030402623003923>
- [15] W. Wang, F. Salvatore, and J. Rech, "Characteristic assessment and analysis of residual stresses generated by dry belt finishing on hard turned aisi52100," *Journal of Manufacturing Processes*, vol. 59, pp. 11–18, 2020. [Online]. Available: <https://www.sciencedirect.com/science/article/pii/S1526612520306289>



- [16] O. Cherguy, F. Cabanettes, S. Han, and J. Rech, "Modeling surface roughness profiles generated by the belt finishing process of a 27mnCr5 carburized steel," *Precision Engineering*, 2024. [Online]. Available: <https://www.sciencedirect.com/science/article/pii/S0141635924000151>
- [17] C. Courbon, F. Valiorgue, C. Claudin, M. Jacquier, F. Dumont, and J. Rech, "Influence of some superfinishing processes on surface integrity in automotive industry," *Procedia CIRP*, vol. 45, pp. 99–102, 2016, 3rd CIRP Conference on Surface Integrity. [Online]. Available: <https://www.sciencedirect.com/science/article/pii/S2212827116006405>
- [18] F. Cabanettes, O. Cherguy, C. Courbon, A. Giovenco, S. Han, and J. Rech, "Towards the prediction of surface roughness induced by the belt finishing process: influence of the workmaterial on the roughness reduction rate," *Procedia CIRP*, vol. 87, pp. 210–215, 2020, 5th CIRP Conference on Surface Integrity (CSI 2020). [Online]. Available: <https://www.sciencedirect.com/science/article/pii/S2212827120302341>
- [19] O. Cherguy, U. Elicegui, F. Cabanettes, S. Han, M. Cici, H. Pascal, and J. Rech, "Effect of abrasive grains size on surface integrity during belt finishing of a 27mnCr5 carburized steel," *Procedia CIRP*, vol. 108, pp. 305–310, 2022, 6th CIRP Conference on Surface Integrity. [Online]. Available: <https://www.sciencedirect.com/science/article/pii/S2212827122005273>
- [20] A. Khellouki, J. Rech, and H. Zahouani, "The effect of abrasive grain's wear and contact conditions on surface texture in belt finishing," *Wear*, vol. 263, no. 1, pp. 81–87, 2007, 16th International Conference on Wear of Materials. [Online]. Available: <https://www.sciencedirect.com/science/article/pii/S0043164807003961>
- [21] A. Hamdi and S. M. Merghache, "Impact of abrasive grit size and mql supply on the surface roughness in belt grinding of a case hardened steel." *Jordan Journal of Mechanical & Industrial Engineering*, vol. 15, no. 5, 2021.
- [22] P. Balland, L. Tabourot, F. Degre, and V. Moreau, "Mechanics of the burnishing process," *Precision Engineering*, vol. 37, no. 1, pp. 129–134, 2013.
- [23] I. Machinery. (July 2, 2020) Effects of ball burnishing process with stainless steel media. [Online]. Available: <https://www.inovatecmachinery.com/blog/ball-burnishing/>
- [24] ECOROLL. Hydrostatic tools - hg series: Overview. [Online]. Available: <https://www.trigon.sk/wp-content/uploads/Hydrostaticke-nastroje.pdf>
- [25] E. Gadelmawlaa, M. Kourab, T. Maksoudc, I. Elewaa, and H. Solimand, "Roughness parameters," *Journal of Materials Processing Technology*, 2002.
- [26] P. Sandoz, G. Tribillon, T. Gharbi, and R. Devillers, "Roughness measurement by confocal microscopy for brightness characterization and surface waviness visibility evaluation." *Wear*, 1996.
- [27] keyence.eu. Param`etres d'amplitude - courbes moyennes. [Online]. Available: https://www.keyence.eu/frfr/ss/products/microscope/roughness/line/tab03_a.jsp
- [28] X. Zhang, V. Suresh, Y. Zheng, S. Wang, Q. Li, H. Lyu, B. Li, and H. Qin, "Surface roughness measurement of additive manufactured parts using focus variation microscopy and structured light system." *In International Manufacturing Science and Engineering Conference*, 2019.



A | Appendix A title

A.1 | Surface Topography Characterization

Table A.1: Confocal Microscopy Roughness values for various parameters without filtering

Surface	Ra	Rz	Rk	Rpk	Rvk	Rsk
SB	0.283	4.483	0.374	0.424	0.274	0.374
FT 0.2	1.507	9.876	0.394	2.169	0.663	0.394
BF 40	0.200	10.279	2.370	2.813	7.467	-1.487
BB 0.05	0.146	6.138	0.429	0.369	0.148	2.167
BB 0.1	0.159	4.451	0.460	0.291	0.182	0.426
BB 0.15	0.239	2.755	0.740	0.366	0.167	0.471
BB 0.2	0.267	2.946	0.909	0.287	0.266	0.128
BB 0.1x5	0.314	3.870	1.015	0.350	0.332	0.036

Table A.2: Confocal Microscopy Roughness values for various parameters without filtering

Surface	Ra	Rz	Rk	Rpk	Rvk	Rsk
SB 0.1	0.265	4.375	0.851	0.409	0.249	0.416
FT 0.2	1.500	9.797	4.122	2.204	0.607	0.409
BF 40	0.207	10.280	0.619	0.259	0.400	-1.55
BB 0.05	0.125	2.683	0.352	0.323	0.620	0.145
BB 0.1	0.134	4.343	0.396	0.254	0.150	0.448
BB 0.15	0.193	2.626	0.618	0.293	0.147	0.476
BB 0.2	0.246	2.844	0.849	0.241	0.205	0.176
BB 0.1x5	0.252	3.765	0.822	0.314	0.260	0.126

Table A.3: Focus Variation Microscopy roughness values for various parameters without filtering

Surface	Ra	Rz	Rk	Rpk	Rvk	Rsk
SB 0.1	0.793	30.135	2.512	0.592	0.868	-0.350
BF 40	0.429	126.514	1.294	0.669	0.764	-65.722
BB 0.05	0.486	27.737	1.571	0.635	0.620	1.785
BB 0.15	0.55	49.759	1.758	0.786	0.702	-0.748
BB 0.2	0.700	45.370	2.169	1.234	0.733	0.805

Table A.4: Focus Variation Microscopy roughness values for various parameters without filtering

Surface	Ra	Rz	Rsk
SB 0.1	0.333	30.133	-0.731
BF 40	0.426	126.507	-65.830
BB 0.05	0.307	27.039	5.598
BB 0.15	0.433	49.725	-1.200
BB 0.2	0.576	45.432	1.428